Supplementary material

Engineering monolayer poration for rapid exfoliation of microbial membranes

Pyne and Pfeil et al.

Materials and Methods

Peptide synthesis and identification. All peptides were assembled on a Liberty-1 microwave peptide synthesizer (CEM Corp.) as peptide amides using solid phase Fmoc/^{t}Bu protocols, HBTU/DIPEA as coupling reagents and Rink amide 4-methylbenzhydrylamine resin (Novabiochem, UK). Fmoc-Ala-OH-3,3,3-d_3 (Sigma Aldrich) was used for the synthesis of GALA d_3-peptides. Following post-synthesis work-up and purification the identities of the peptides were confirmed by analytical RP-HPLC and MALDI-ToF mass spectrometry. ^{15}N-tilamin (KA*RL*A*KLRA*RL*YRL*KARL*A*RL) was from Eurogentec. MS $[M + H]^+$: tilamin, *m/z* 2537.2 (calculated), 2537.4 (found); d_3-tilamin, *m/z* 2540.2 (calculated), 2540.8 (found); ^{15}N-tilamin, *m/z* 2545.3 (calculated), 2545.8 (found); *N*-carboxyfluorescein-βAla-tilamin, *m/z* 2965.5 (calculated), 2964.1 (found); $[M - H]^-$: non-AMP, *m/z* 2370.2 (calculated), 2370.9 (found).

High performance liquid chromatography. Analytical and semi-preparative gradient RP-HPLC was performed on a JASCO HPLC system using Vydac C18 analytical (5 μm) and semi-preparative (5 μm) columns. Both analytical and semi-preparative runs used a 10− 60% B gradient over 50 min at 1 mL/min and 4.7 mL/min respectively with detection at 230 and 220 nm. Buffer A - 5% (vol/vol) and buffer B – 95% (vol/vol) aqueous CH_3CN, 0.1% TFA. For non-AMP peptide, both analytical and semi-preparative runs were performed using a 40-90% B gradient. Tilamin eluted at 58% CH_3CN; t_R = 12 min.

Minimum inhibitory concentrations assay. Minimum inhibitory concentrations (MICs) were determined by broth microdilution on *P. aeruginosa*, *E. coli*, *S. aureus*, *M. luteus*, *B. subtilis*, *S. enterica* and *E. faecalis* according to the Clinical and Laboratory Standards Institute. Typically, 100 μL of 0.5–1 × 106 CFU per ml of each bacterium in Mueller Hinton media broth (Oxoid) were incubated in 96-well microtiter plates with 100 μL of serial twofold dilutions of the peptides (from 100 to 0 μM) at 37 °C on a 3D orbital shaker. The absorbance was measured after peptide addition at 600 nm using a Victor 2 plate reader (Perkin-Elmer). MICs were defined as the lowest peptide concentration after 24 h at 37 °C. All tests were done in triplicate and results are summarised in Table S1.

Haemolysis assay. Haemolysis was determined by incubating a 10% (vol/vol) suspension of human erythrocytes with peptides. Erythrocytes were rinsed four times in 10 mM phosphate buffer saline (PBS), pH 7.2, by repeated centrifugation and re-suspension (3 min at 3000 × g). Erythrocytes were incubated at room temperature for 1 h in either deionized water (fully haemolysed control), PBS, or with peptide in

PBS. After centrifugation at 10,000 × g for 5 min, the supernatant was separated from the pellet, and the absorbance was measured at 550 nm. Absorbance of the suspension treated with deionized water defined complete haemolysis. The values given in Table S1 correspond to concentrations needed to kill a half of the sample population (50% lysis of human erythrocytes) and are expressed as median lethal concentrations—LC_{50}. All tests were done in triplicate and results are summarised in Table S1.

Bacterial viability LIVE/DEAD® BacLight™ assays. *E. coli* culture (1 mL) was centrifuged to give a cell pellet, which was washed twice with 10 mM phosphate buffer (pH 7.4) before being reconstituted in the same buffer to give OD600nm = 0.008. A 100-µL aliquot of the solution was dispensed in an eight-well glass chamber (LabTek) with LIVE/DEAD® BacLight™ bacterial viability kit (Invitrogen). The chambers with surface-settled bacteria (20 min) were mounted on a confocal microscope (Olympus) equipped with an incubation chamber at 37 °C. SYTO®9 and PI fluorescence emission was monitored at 515 nm and 625 nm, respectively, at different time points for 45 min after the addition of peptides. Recorded images (XY) were analyzed using Fiji software to plot the number of dead bacteria as a percentage of the total number of cells (taken as 100% for each point). The data is shown in Fig S1.

Atomic force microscopy of bacteria in water. *E. coli* were grown up overnight in LB at 37°C and 250 rpm. After incubation, the bacteria were sedimented (5000 rpm, 1 min), washed (3x) and re-suspended in water. The bacteria were diluted down to a concentration of ~10^6 CFU/mL. Washed bacteria were incubated on glass coverslips coated with 0.01% poly-L-lysine (Sigma-Aldrich, St Louis, USA) for 30 min at room temperature. The coverslips were then washed in a stream of Milli-Q® water and left with a water droplet. Care was taken not to allow the bacteria to dry out. Topographic images of *E. coli* cells in liquid were recorded on a Nanowizard III AFM with an UltraSpeed head (JPK, Germany) operated in intermittent contact mode at room temperature. The AFM probes used for experiments in liquid were FastScan-D (0.25 N/m) (Bruker AXS, CA, USA). Images were processed using Gwyddion (http://gwyddion.net/) for 0^{th} order line by line flattening to centre data, and 1^{st} or 2^{nd} order plane fitting to remove tilt or bow. High resolution scans of *E. coli* surfaces were processed using an additional 2^{nd} order polynomial fit to remove the curvature of the surface. Cross-section measurements were carried out using Gwyddion and plotted using Origin (OriginLab, MA, USA). The data is shown in Fig 3, S2, S3.

Fluorescence imaging of bacteria in water. Propidium iodide (PI) stain (Invitrogen, CA, USA) was used to stain dead bacteria in water at a concentration of 5µg/ml at room temperature. Fluorescent images were taken using an Andor Zyla 5.5 USB3 fluorescence camera mounted on an Olympus IX 73 inverted optical microscope. PI fluorescence emission was monitored at 625 nm, and peptide fluorescence was monitored using an appropriate filter. Images were processed using ImageJ (U. S. NIH, Bethesda, Maryland, USA, http://imagej.nih.gov/ij/). The data is shown in Fig S2C.

Unilamellar phospholipid vesicle preparation. 1,2-dilauroyl-sn-glycero-3-phosphocholine (DLPC) with 1,2-dilauroyl-sn-glycero-3-phospho-(1'-rac-glycerol) (DLPG) and (1-palmitoyl-2-oleoyl-sn-glycero-3-phosphocholine (POPC) with 1-hexadecanoyl-2-(9Z-octadecenoyl)-sn-glycero-3-phospho-(1'-rac-glycerol) (POPG)) lipids used for vesicle construction were from Avanti Polar Lipids (Alabaster, USA). DLPC and POPC were used as mammalian model membranes, and DLPC/DLPG (3:1, molar ratios) and POPC/POPG (3:1, molar ratios) were used as bacterial model membranes. The lipids were weighted up, dissolved in chloroform-methanol (2:1, vol/vol), dried under a nitrogen stream and then under vacuum to form a thin film. The film was hydrated in 10 mM phosphate buffer (pH 7.2) with shaking (1 h, 220 rpm) and bath sonicated. The obtained suspension was extruded using a hand-held extruder (Avanti Polar lipids) (twenty times, polycarbonate filter, 0.05 μm) to give a clear solution containing small unilamellar vesicles, which were analysed (50 nm) by photon correlation spectroscopy. For cwEPR experiments lipid films were obtained with spin labelled phosphatidylcholine (PCSL; 0.5% molar ratio of total lipid), followed by five freeze-thaw cycles to ensure unilamellar vesicle formation. For NMR experiments the lipid films were hydrated in 10 mM phosphate buffer prepared with deuterium-depleted water.

Photon correlation spectroscopy. Vesicles were re-suspended to a final concentration of 1 mg/mL and were analysed on a Zetasizer Nano (ZEN3600; Malvern Instruments). Dynamic light scattering batch measurements were carried out in a low volume disposable cuvette at 25 °C. Hydrodynamic radii were obtained through the fitting of autocorrelation data using the manufacturer's software, Dispersion Technology Software (DTS version 5.10).

Circular and linear dichroism spectroscopy. All CD spectra were recorded on a JASCO J-810 spectropolarimeter fitted with a Peltier temperature controller. All measurements were taken in ellipticities in mdeg and converted to molar ellipticities ([θ], deg $cm^2 \cdot dmol^{-1}$ res^{-1}) by normalizing for the concentration of peptide bonds (Fig S4A). Aqueous peptide solutions (300 μL, 30 μM) were prepared in filtered (0.22 μm), 10 mM phosphate buffer, pH 7.4. CD spectra recorded in the presence of synthetic membranes are for lipid-peptide (L/P) molar ratios of 100. Solution-phase flow LD spectra were recorded on a Jasco-810 spectropolarimeter using a photo-elastic modulator 1/2 wave plate, and a microvolume quartz cuvette flow cell with ~0.25 mm annular gap and quartz capillaries (all from Kromatec). Molecular alignment was achieved through the constant flow of the sample solution between two coaxial cylinders: a stationary quartz rod and a rotating cylindrical capillary. LD spectra were acquired with laminar flow obtained by maintaining a cell rotation speed of 3000 rpm and processed by subtracting nonrotating baseline spectra. LD spectra recorded in the presence of synthetic membranes were prepared at a 100 L/P molar ratio (2 mM total lipid, 15-30 μM peptide). The data is shown in Fig S4.

Sample preparation for surface imaging in air. Ozone-cleaned silicon substrate 1-cm^2 squares with oxide layer thickness of 9 nm (University Wafer) were submerged into a solution containing DLPC/DLPG

(3:1, molar ratio) AUVs (0.4 mg/mL) with shaking (2 h) to enable the deposition of the lipid bilayer on the surface. The substrates were then plunged into a dish of water and kept with shaking (3 min x 3) to remove AUV excess. The surface lipid bilayer was then placed into a dish and treated with a 10-μM peptide solution (10 mL) for 15 min, followed by washing to remove peptide excess (this step was omitted for control samples that did not require peptide treatment). The substrate without drying was transferred into a 2-mL container filled with water, which was plunged into a chamber with liquid nitrogen to quickly freeze the entire sample. The lid of the container was replaced with a perforated lid, and the sample was freeze-dried. The same procedures were performed for both supported lipid-bilayer and bare substrates. The data is shown in Fig 4A, S5B.

In-air atomic force microscopy imaging. Topographic, amplitude, phase and z-sensor images were recorded using tapping mode AFM on a Cypher Instrument (Asylum Research, UK). All AFM images were flattened with a first-order line-wise correction fit. AFM tips were super-sharp silicon probes (SSS-NCHR Cantilever, Nanosensors, Switzerland) with resonant frequency~330 kHz, tip radius of curvature < 5 nm, and force constant 42 N/m. Images were processed using proprietary SPIP software, version 5.1.3.

Preparation of supported lipid bilayers for AFM in aqueous solution. Supported lipid bilayers were formed on mica as described elsewhere[34] from a vesicle solution of 4 mg/ml DLPC/DLPG (3:1, molar ratio) and for POPC/POPG (3:1, molar ratio) SLBs. The vesicle solution was incubated on the mica for 60 minutes in 150 mM NaCl, 20 mM HEPES pH 7.2, with 20 mM $MgCl_2$ and 20mM $CaCl_2$. After adsorption, the solution was washed three times with buffer, to remove unfused vesicles from solution. Peptides were introduced into the 100-μl fluid cell (Bruker AXS, USA) and diluted in the existing buffer solution (150 mM NaCl, 20 mM HEPES pH 7.2) to the final concentration stated. Mica disks (Agar Scientific, Stansted, UK) were glued to a metal puck, and freshly cleaved prior to lipid deposition.

Atomic force microscopy in aqueous solution. Topographic images of supported lipid bilayers in water were recorded on a Multimode 8 AFM (Bruker AXS, CA, USA) operated in PeakForce Tapping mode at PeakForce frequency 2 kHz, PeakForce amplitude 10 nm, at a set-point of 40-60 pN. The AFM probes used for experiments in liquid were Biolever Mini (0.08 N/m) (Olympus, Japan) and MSNL-E, MSNL-F (0.1, 0.6 N/m) (Bruker AFM probes, CA, USA). Images were processed using NanoScope Analysis (Bruker AXS, CA, USA) for 0^{th} order line by line flattening to centre data, and 1^{st} or 2^{nd} order plane fitting to remove tilt or bow. Cross-section measurements were carried out using NanoScope Analysis or Gwyddion (http://gwyddion.net/) and plotted using Origin (OriginLab, MA, USA). The data is shown in Fig 4B, S5A & C, S6, S7, S8D, S9.

Quantifications of pore size dynamics (depths and widths) were performed by further analysis in Gwyddion. The data was processed as detailed above and then masked to select areas below a given threshold (Fig S7 and S9). In each image the masked data (pores) is shown in red, with the specific used

threshold labelled on the image. Statistical grain analysis was performed on the masked data to show the mean values of each pore and plotted using Origin (OriginLab, MA, USA).

Nanoscale secondary ion mass spectrometry. A CAMECA NanoSIMS 50 instrument was used to acquire chemical and isotopic distributions with spatial resolution better than 100 nm. The instrument uses a 16 keV primary $^{133}Cs^+$ beam to bombard the sample surface and collects and analyses selected secondary negative ions. For this experiment, $^{12}C^{14}N^-$ and $^{12}C^{15}N^-$ secondary ions were collected to show the distribution of ^{15}N-labelled tilamin on the sample surface. This data is presented as ratio images ($^{12}C^{15}N^-$ /$^{12}C^{14}N^-$) over areas of 6 by 6 µm containing 256 by 256 pixels collected with the smallest aperture (D1=4) to achieve high lateral resolution. The data were collected without preliminary $^{133}Cs^+$ implantation to avoid sputtering away the thin samples. The images were processed using OpenMIMS software (MIMS, Harvard University; www.nrims.harvard.edu). The data is shown in Fig 4C.

Tilamin cross-linking. Disuccinimidyl suberate (DSS) (Thermo Scientific Pierce, Germany) was used as a cross-linking agent in all experiments. 50-fold molar excess of the reagent was incubated with tilamin for 90 min. Before the reaction, tilamin (400 µM for SDS polyacrylamide gel electrophoresis; 100 µM for LC-MS analysis) was pre-incubated in 10 mM MOPS buffer, 10 mM NaCl (pH 8) with shaking for 30 min without and with unilamellar vesicles (20-fold molar excess of total lipid: unilamellar vesicles were prepared in incubation buffer at a size of 0.1 µm). After the reaction, samples were lyophilized, dissolved in 300 µL acetonitrile/water (45%/55%; vol/vol, with 0.1 % TFA) and purified (150 µL) by an Elite LaChrom liquid chromatography (VWR–Hitachi, Darmstadt, Germany) using a BioSep-SEC-S2000 column (5 µm, 150 Å, 300 x 7.8 mm, Phenomenex, USA). Isocratic elution using acetonitrile/water (45%/55%; vol/vol, with 0.1 % TFA) at a flow rate of 1 mL/min was monitored at 215 nm over 20 min. Individual fractions were collected for mass-spectrometry and SDS analyses. The data is shown in Fig S8A-C.

Liquid chromatography mass spectrometry: The collected fractions (0.5 mL) were lyophilized and dissolved in 30 µL acetonitrile/water (45%/55%; vol/vol; with 0.1 % formic acid). 4 µL of each sample was analysed on an Agilent 1200 series LC instrument (Agilent Technologies, USA) using a Jupiter C4 column (5 µm, 300 Å, 150 x 2.0 mm, Phenomenex, USA) and 5-90% B gradient over 45 min at a flow rate of 0.2 mL/min (A, water with 0.1 % formic acid; B, acetonitrile with 0.1 % formic acid). Mass analysis was performed on an Orbitrap Elite Hybrid Ion Trap mass spectrometer (Thermo Fisher Scientific; Waltham, MA, USA) operated in positive electrospray ionization mode at a minimum resolution of 60000. Full scans were recorded from m/z 400 to 2000 and de-convolved using proprietary XCalibur 2.2 SP1 software (Thermo Fisher Scientific, USA). The cross-linking reagent requires <11.4 Å proximity between linked amines, while an average intermolecular distance of ~160 Å is expected in solution under the same conditions. Assuming that all reactive sites within each peptide monomer reacted (24 sites in a hexamer),

the minimum theoretical mass is based on the total of complete cross-links (12 in a hexamer), whereas a maximum theoretical mass derives from the minimum number of cross-links (5 in a hexamer) combined with the remaining reactive sites[39] modified with one DSS molecule each, with unreacted DSS moieties quenched by water. These mass ranges are indicated by orange bars in Fig. S8C.

SDS polyacrylamide gel electrophoresis: The lyophilized SEC fractions (3.5 mL) were dissolved in 100 µL Tricine-SDS sample buffer (1x) and heated for 2 min at 85 °C before loading 8 µL of each sample onto Novex 16 % Tricine mini-gels. Mark12 (M12) unstained protein marker (4 µL) was used for molecular weight estimation. After filling the XCell SureLock mini cell with Tricine SDS running buffer (1x) electrophoresis was performed at a constant voltage of 125 V for 90 min. Finally, gels were stained with SimplyBlue^{TM} SafeStain using proprietary protocols. All reagents and protocols were from Invitrogen.

Giant unilamellar vesicles preparation and imaging. POPC/POPG (3:1, molar ratio) powder was dissolved in chloroform, dried under vacuum to form a thin film, which was then dried under ultrahigh vacuum for 3 h. The film was hydrated in 1 M sorbitol (1 mL) containing sulforhodamine B (2 µM). The obtained suspension was sonicated for 30 sec at room temperature and diluted (1/1000) in PBS, and an aliquot (100 µL) was deposited onto an 8-well Lab-Tek^{TM} chamber with CellMask™ Deep Red dye (1/2000 dilution). After a 5-min incubation to allow GUVs to settle down, tilamin or carboxyfluorescein-labelled tilamin was added to the final concentration of 10 µM (L/P 100). Fluorescence was monitored for 45 min by a confocal laser scanning microscope (CLSM) (FV-1000, Olympus) using appropriate filters. Images were processed by Imaris 6.2.1 software (Bitplane). The data is shown in Figs 5 and S10.

Solid-state nuclear magnetic resonance spectroscopy.

Sample preparations of mechanically aligned membranes: four tilamin sequences, each deuterated at a single alanine, were used (Fig 1A). Each peptide was dissolved together with (i) DLPC/DLPG (3:1, molar ratio) or (ii) POPC/POPG (3:1, molar ratio) in chloroform:methanol:water (45:45:10) at the required molar ratio. ~ 3 mg/cm^2 lipids were applied to ultrathin microscope cover glass slides with dimensions 5.7 x 11 mm (Paul Marienfeld GmbH & Co KG, Germany). The peptide lipid mixture was air-dried at room temperature for 1 h and followed by additional drying in vacuum for 12 h. The lipid films were rehydrated at 96% relative humidity for 8 h at 37 °C, the slides were stacked on top of each other and hydrated for an additional 24 h. The sample was inserted into a glass sample cell and sealed.[S1] Lipid orientation was determined using ^{31}P NMR with ^{1}H decoupling on a 400 MHz Bruker Avance wide bore spectrometer using a double resonance probe, which was modified with a flattened coil.

Static ^{2}H ssNMR: experiments were run on 800 MHz Infinity plus wide bore spectrometer (Magnex; Varian) using a static flat coil low-e HX probe.[S2] The deuterium spectra were obtained using a quadrupolar echo pulse sequence. Measurements were performed at 20 °C and samples were allowed to equilibrate (30 min) before each measurement. The quadrupolar echo ^{2}H experiments were performed at a frequency

of 122.78 MHz with a 4 μs 90° pulse, a 60 μs pulse delay followed by a relaxation delay of 100 ms. A total of 400k-600k scans was collected for each spectrum. The FID was left shifted to the echo maximum prior Fourier Transformation and an exponential line broadening of 100 Hz was applied.[43]

Geometric analysis of labelled alanines (GALA): distinct quadrupolar splittings resolved for each of the positions were related to give a bond vector showing the relative orientation of the C_α-C_β side-chain bonds[43] (Fig. S11A). Characteristic Pake doublets gave comparable values for both lipid compositions (Tables S2-S4, Fig 6A). The quadrupolar splittings were fitted to an overall tilt and rotational peptide angle using relationships described elsewhere,[S3] where the 0° rotation was defined as 180°, or opposite, a central residue in the hydrophobic cluster (Fig S11B):

$$\Delta\nu_q = \frac{1}{2}\ \Delta\nu_{q(theoratical)}\ [3cos^2\beta(\cos\tau - \sin\tau\cos\delta\tan\beta)^2 - 1]$$

To exclude the impact of heterogeneous orientation on the obtained tilt angles and to confirm sample preparation and membrane alignment, the spectra were deconvoluted to individual components providing their full analysis (Table S3 and Fig S12). ^{31}P spectra are included to demonstrate good lipid alignment for all samples with minor powder components of <10% in ^{2}H spectra (Table S3). This is also to reflect on that pattern is inherent to such samples as lipids curve around the edges of aligned bilayers as well as small unaligned proportions in a large sample[44,S1] (Fig S12).

To obtain the final peptide orientation, the following equation was minimised (see RMSD plots in Fig S13B):

$$RMSD = \sqrt{\frac{\sum((data) - (expected))^2}{n}}$$

The alanine side chain of a straight α-helix was described by Euler angles [0.0; 55.2; 0.0].[S4] A maximum quadrupolar splitting for deuterated methyl groups of 84 kHz and corresponding dynamics were assumed.[S5] Due to the sign ambiguity of quadrupolar splittings absolute values were used for the analysis and spectral simulations.

Static ^{15}N NMR: a single ^{15}N enriched label was incorporated at the central tyrosine residue of tilamin, which allowed for confirmation of the ^{2}H NMR constraints. ^{1}H decoupled cross polarization experiments were performed on a 400 MHz Bruker Avance wide bore spectrometer.[S6] A spin-lock time of 1000 ms and a recycle delay of 2.5 s at an observer frequency of 40.55 MHz were used. A typical experiment would allow for ca. 200 000 acquisitions, 1024 data points and a spectral width of 50 kHz. The FID was left shifted and line broadened before Fourier Transformation. Spectra were referenced to $^{15}NH_4Cl$ powder.

The data was analysed according to the following relationship,[S7] with the principle chemical shift tensors for tyrosine σ_{11}, σ_{22} and σ_{33} to be 55.1 ppm, 77.1 ppm and 209.3 ppm respectively:[S8]

$$\sigma_{zz} = \sigma_{11} sin^2\theta cos^2\phi + \sigma_{22} sin^2\theta sin^2\phi + \sigma_{33} cos^2\theta$$

Simulation of NMR spectra: the software library *"Spinach"* was used to simulate static oriented ^{2}H NMR spectra.[S9] Simulation parameters are in accordance with NMR parameters: a B_1 field of 18.8 Tesla, sweep width of 100 kHz and a total of 1024 points. The simulated FID was zero filled by 1024 points and an apodization of 80 Hz was applied before Fourier Transformation. The real part of the spectrum was plotted. Similar to the GALA analysis a straight alpha helix was assumed that was described by three Euler angles assuming a side chain tilt of 55.2°.[S4] Due to the sign ambiguity of quadrupolar splittings the simulated and experimental values were fitted as absolute values.

The simulated spectra were analysed by minimizing the following function (see RMSD plots and spectra in Fig S14A, B):

$$RMSD = \sqrt{\frac{\sum((data) - (expected))^2}{n}}$$

A total of 60 data points were simulated in each dimension leading to a total of 14 400 simulated spectra and a step size of 3° in each dimension. A best fit with an RMSD of 1.1 kHz was achieved. The data for a range of rotational and tilt angles for four tilamin peptides is represented by a contour plot of all RMSD values (Fig S13B, S14A).

Static ^{2}H ssNMR of head group and acyl chain deuterated lipids: for headgroup ^{2}H experiments, peptide was added to the lipid vesicles in phosphate buffer (pH 7.2) at 100 L/P molar ratios in the palmitoyl (POPC/POPG, 3:1, molar ratio) membranes. Static ssNMR experiments were done on 800 MHz Infinity plus wide bore spectrometer, equipped with a 4 mm HXY probe at 25 °C. Spectra were acquired at 122.78 MHz using a quadrupole echo sequence with a 4 μs 90° pulse, a 50 μs refocusing delay and a recycle delay of 0.5 s. The spectra were subsequently left shifted to the echo maximum and de-Paked.[S10] Mechanically aligned samples for acyl chain deuterated lipids were prepared as described before. Spectra were recorded using a flat coil static low-e probe with parameters outlined before. Smoothed acyl chain order parameter profiles (S_{seg}) were calculated.[S11]

Note: A constant error estimate of +/- 2 kHz and +/- 3 ppm for quadrupolar splittings and ^{15}N were considered for all NMR spectra.[S12] The data is shown in Fig S13, S16 and S18.

Continuous wave electron paramagnetic resonance (cwEPR). Peptide (10 mM phosphate buffer pH 7.2) was added to both POPC/POPG and DLPC/DLPG (3:1, molar ratio) at the required L/P molar ratio – 100, 25 and without peptide. For all three ratios phosphatidylcholine with the nitroxide spin label at positions 5 (5-PCSL) and 12 (12-PCSL) of the acyl chain was used. The samples were loaded in 100 μL sealed-off capillaries and analysed on a Bruker EMX X-band cwEPR spectrometer at a sweep width of 150 gauss, a mod. amp of 1g and a centre field at 3297 gauss. Spectra obtained are over 18 °C – 40 °C

(+/-0.5 °C) temperature ranges. Samples were allowed to equilibrate at a set temperature prior to each measurement. Each temperature point is an average of three scans.

Calculation of order parameters (S^{eff})

The order parameters were calculated as described in,[S13] where the molecular axes of the spin label are represented by the hyperfine splittings A_{zz}, A_{yy} and A_{xx}. The structural factor S^{eff} was calculated as follows:

$$S^{eff} = \frac{A_{II} - A_{\perp}}{A_{zz} - (\frac{1}{2})(A_{xx} + A_{yy})} \times \frac{a'_0}{a_0}$$

where

$$a'_0 = \left(\frac{1}{3}\right)(A_{zz} + A_{yy} + A_{xx}) \quad a_0 = \left(\frac{1}{3}\right)(A_{II} + 2A_{\perp})$$

The principal hyperfine splittings for A_{zz}, A_{yy} and A_{xx} in type II spin labels were previously characterised as 5.9, 5.4 and 32.9 Gauss, respectively.[S14] The data is shown in Fig S17.

Molecular dynamics simulations. Molecular dynamics simulations were performed using the CHARMM36 force field using chloride counter ions for charge neutralization. The initial helical configuration was obtained using the XPlor-NIH structure determination algorithm (http://nmr.cit.nih.gov/xplor-nih/). DLPC/DLPG (3:1, molar ratio) membranes were constructed with dimensions of 12 × 12 nm and simulated with a semi-isotopic moles, pressure, and temperature (NPT) ensemble with equilibrations of 20-40 ns. Production runs were then performed for ~100-500 ns.

The angle of the peptide was measured by calculating a vector in the direction of the helical axis, and subsequently calculating the angle of this vector relative to the plane of the membrane. Throughout the trajectory, these orientation angles were then binned into 1 degree intervals to produce histograms of the angles adopted by the helix in the simulation. Radial density functions (RDFs) were produced using the GROMACS g_rdf tool. For RDFs between lysine and phospholipids, the atoms used were the lysine side-chain N atom and the phospholipid P atom. For arginine, the side-chain terminal C atom was used again with the phospholipid P atom. In tyrosine, the hydroxyl O atom was used with the phospholipid P atom. Data were normalized to account for the 3:1 PC:PG ratio before plotting.

The tilamin pore structures were built using X-PLOR scripting, modelling α–helical tilamin protomers with a C-amidated terminal, and forming a symmetrical octameric pore consisting of eight helices. These structures were converted to coarse grained (CG) representation embedded into a POPC/POPG (3:1, molar ratio) membrane and solvated in the presence of 150 mM NaCl, using the CHARMM-GUI Martini webserver.[S15] The force field Martini 2.2 was employed and, after careful equilibration, 10 μsec of production MD trajectory were reached. On the other hand, starting from a frame of the CG simulation rep-

resenting an incipient opening of the pore, an atomistic (AT) model was generated with the same membrane composition employing the CHARMM-GUI Martini webserver.[S16] After equilibration, 70 nanoseconds of AT MD simulation were run. In both CG and AT simulations, L/P ratio was ~70. GROMACS 5.1[S17] and VMD[S18] software were used for trajectory analysis. The data is shown in Fig 5C, S19, S20A.

Fluorescence spectroscopy. Tyrosine fluorescence was measured using a Varian Cary Eclipse fluorescence spectrometer (Agilent Technologies) using excitation and emission slits of 5 nm. Samples were excited at 274 nm and the emission spectra were measured between 280-400 nm. The data is shown in Fig S20B.

Tables and Figures

Table S1. Biological activities of peptides used in the study

Cell	peptide[a]				
	tilamin	amhelin	cecropin B	daptomycin	polymyxin B
	Minimum inhibitory concentrations, μM				
P. aeruginosa (ATCC27853)	4.0	12.3	1.6	>100	<1
S. aureus (ATCC6538)	8.8	>50	>100	7.7	≤50
E. coli (K12)	10.2	3.0	<1	>100	<1
B. subtilis (ATCC6633)	<1	6.2	>50	7.7	1.5
S. enterica (ATCC700720)	3.1	6.2	3.1	>50	<1
E. faecalis (OG1X)	3.1	6.2	25	>100	>100
M. luteus (ATCC7468)	<1	7.1	<1	15.4	<1
	(LC_{50})[b], μM				
Human erythrocytes	10^4	12 x 10^3	8.3 x 10^3	10^3	N/D

[a]non-AMP was inactive (>>250 μM); [b]median (50%) lethal concentration calculated from the actual percentage of lysed bacteria populations at 500 μM. Red, blue and green denote Gram negative, Gram positive and Gram variable bacteria, respectively. N/D – non-detectable. All tests were done in triplicate.

Table S2. Quadrupolar splittings[a] obtained for Ala-d_3 tilamin in reconstituted membranes.

Tilamin	Quadrupolar splitting ($\Delta\nu_Q$) in kHz		
	POPC/POPG[b] L/P 25	POPC/POPG[b] L/P 100	DLPC/DLPG[b] L/P 100
-5d_3	46.3	48.1	47.3
-9d_3	19.1	23.1	23.0
-16d_3	38.5	40.8	41.5
-19d_3	8.7	10.8	14.0

[a]quadrupolar splittings are absolute values due to sign ambiguity; [b]3:1, molar ratio

Table S3. Deconvoluted components and corresponding line widths of selectively deuterated tilamin in POPC/POPG (3:1; molar ratio) at L/P 25 (Fig 6). The deconvolution process is illustrated in Fig S12.

Tilamin	Deconvoluted component	Line width, kHz	Proportion, %
-5d_3	peptide	2.2	90.4
	powder	-	-
	isotropic	0.3	9.6
-9d_3	peptide	2.3	77.9
	powder	2.7	8.2
	isotropic	0.5	13.9
-16d_3	peptide	2.0	78.0
	powder	1.6	7.8
	isotropic	0.2	14.2
-19d_3	peptide	2.1	78.6
	powder	2.4	10.0
	isotropic	0.4	11.4

Table S4. Possible solutions for tilt ensemble angles as observed in the RMSD analysis (see Fig S13).[a]

tilamin	Tilt and rotational angles (in degree)			
	POPC/POPG (3:1, molar ratio)		DLPC/DLPC (3:1, molar ratio)	
	tilt	rotation	tilt	rotation
solution 1	111	115	112	119
solution 2	71	90	70	91
solution 3	88	15	88	15

[a]solution 3 is given despite no overlap, but close proximity; [b]3:1, molar ratio. For ^{2}H constraints only regions with an RMSD of <4 kHz were considered.

Table S5. Comparison of simulated and experimental quadrupolar splittings tilamin in POPC/POPG (3:1; molar ratio) (Fig S13).

Tilamin	Simulated $\Delta\nu_Q$ (kHz)	Experimental $\Delta\nu_Q$ (kHz)
-9d₃	18.8	19.1
-16d₃	37.9	38.5
-5d₃	47.1	46.3
-19d₃	9.9	8.7

[a]quadrupolar splittings are absolute values due to sign ambiguity

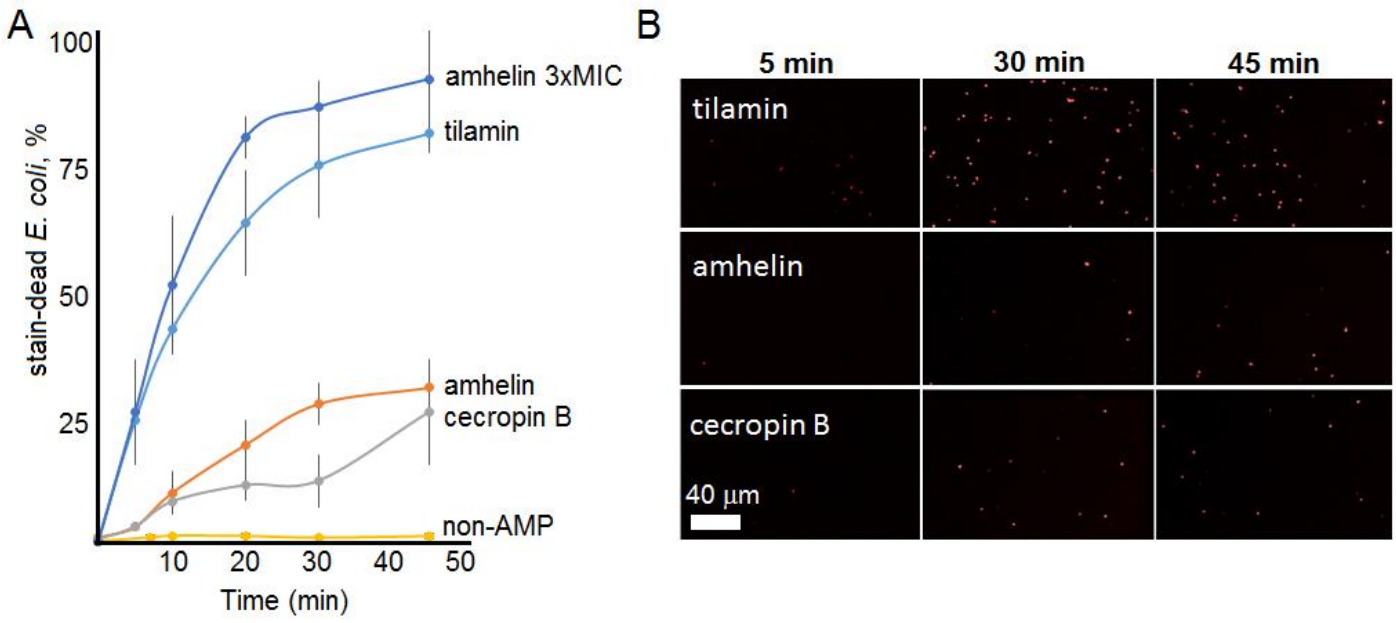

Fig. S1. Antimicrobial kinetics of studied peptides. (A) Average numbers of stain-dead *E. coli* cells incubated with tilamin (blue), amhelin (orange), cecropin B (grey) at MICs, amhelin at 3xMIC (dark blue) and the non-AMP at 10 µM (yellow) as a function of time. The data represent mean values ± s. d. (B) Fluorescence microscopy images of PI-stained *E. coli* cells.

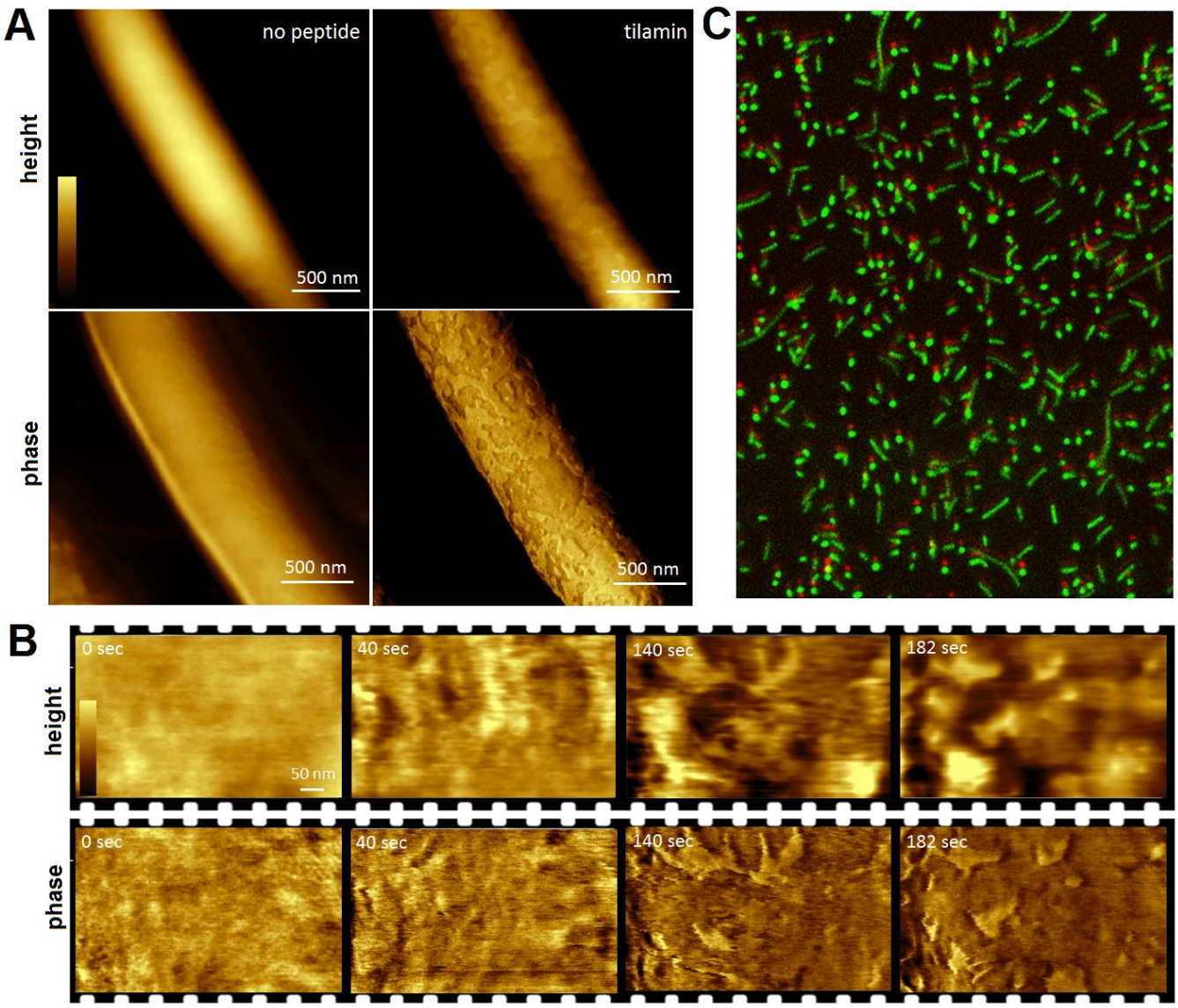

Fig S2. Membrane-permeabilizing activity of tilamin. (A) Topographic (height) and phase AFM images of live *E. coli* in water without peptide (left) and after the first 780-sec incubation with tilamin (right). Colour scale: 140 nm. (B) High resolution topography and phase images of *E. coli* during incubation with tilamin. Time-point labels indicate time since injection. Colour scale: 12 nm. (C) A composite of fluorescence micrographs (488 nm) obtained for *E. coli* at 780 sec of incubation with fluorescein-labelled tilamin (green) and after being subjected to PI-staining (red). Incubation conditions: 3.5 μM, pH 7.4, rt.

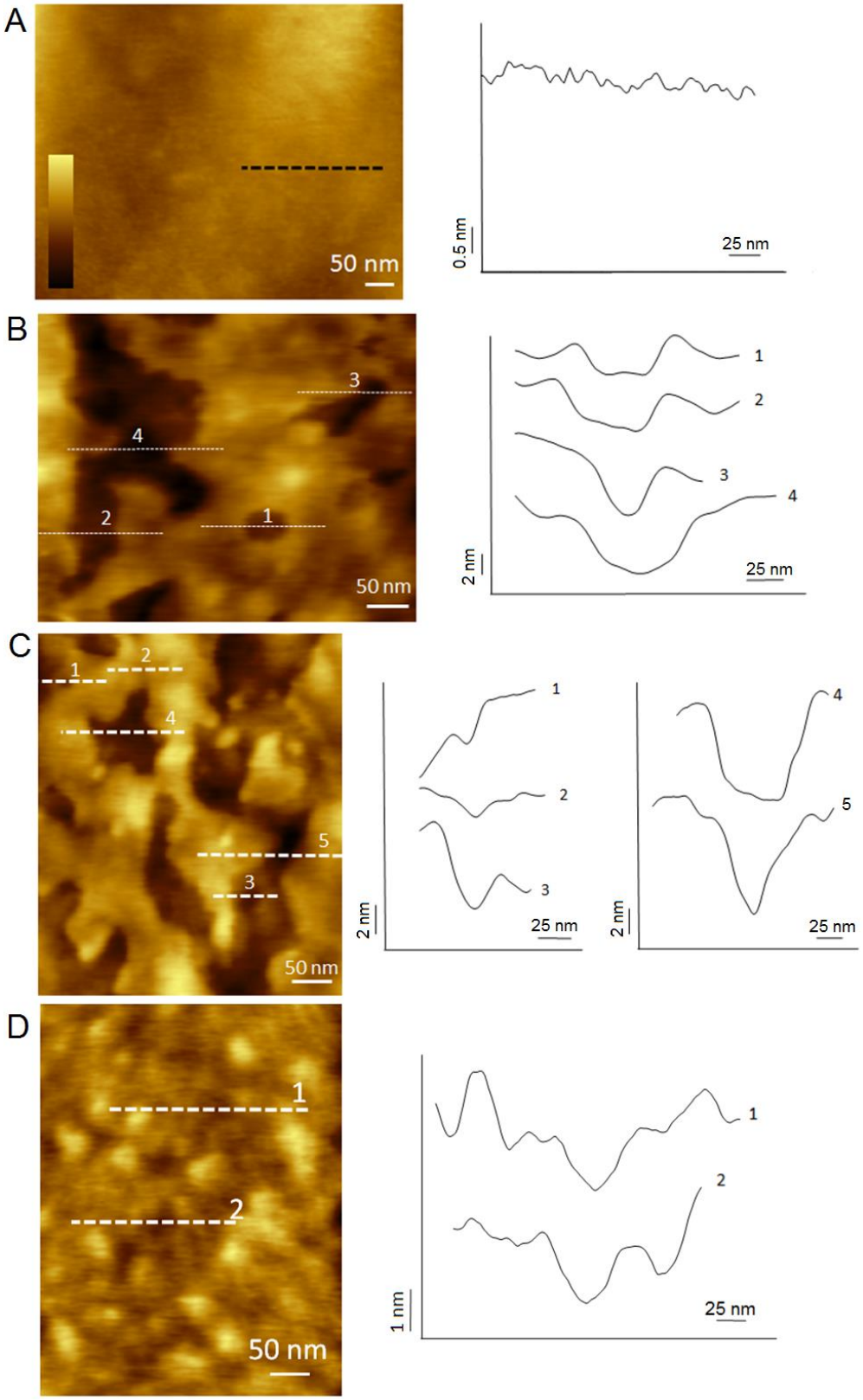

Fig. S3. Poration by tilamin. High resolution images of *E. coli* (A) without peptide treatment and (B-D) during incubation with tilamin taken at different time-points: (B) 60 min, (C) 20 min and (D) 8 min post-injection. Cross-sections along the highlighted lines show an unperturbed bacterial surface (A); profiles of monolayer depths (lines 1 in B and C; line 2 in C; lines 1,2 in D), developing holes (lines 2-4 in B; 3 in C) and lesions piercing through the outer cell-wall layer (lines 4, 5 in C). Colour scales: 18 nm (A, B), 12 nm (C), 6 nm (D). Incubation conditions: 3.5 μM, pH 7.4, rt.

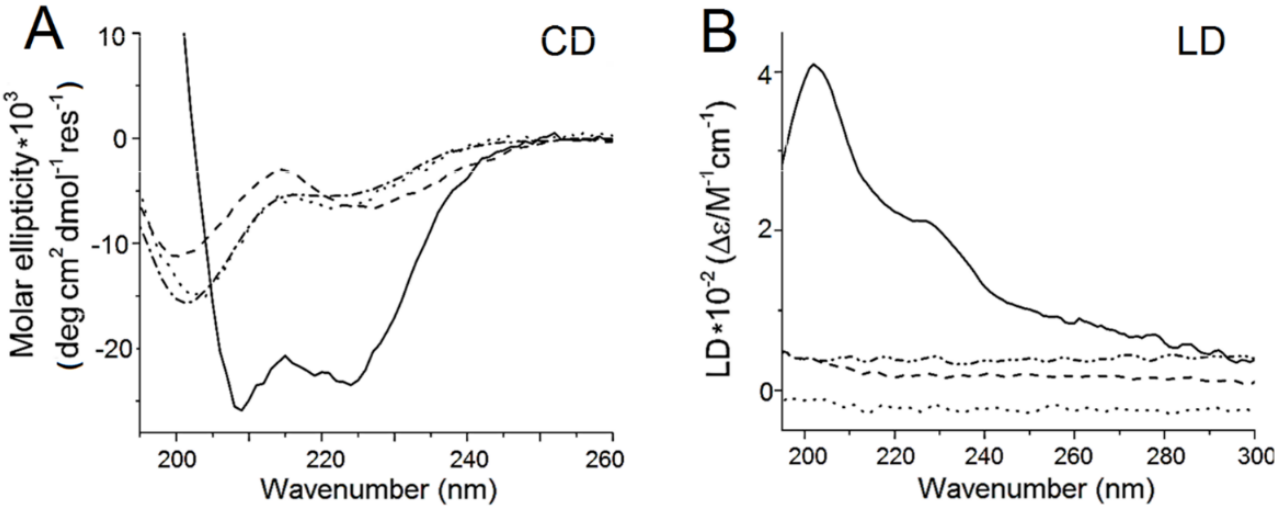

Fig. S4. Peptide folding. (A) Circular dichroism (CD) spectra for tilamin in the DLPC/DLPG (3:1, molar ratio) AUVs (solid line), DLPC (dotted line) and phosphate buffer (dash-dotted line) and for non-AMP in the DLPC/DLPG (3:1, molar ratio) AUVs (dashed line). Peptides were at 30 μM, at L/P 100 molar ratios. (B) Linear dichroism (LD) spectra for tilamin in DLPC/DLPG) (3:1, molar ratio) AUVs (solid line) and DLPC (dotted line), and for non-AMP in DLPC/DLPG (3:1, molar ratio) AUVs (dashed line) and in DLPC (dash-dotted line). Spectra comprise a flattened maximum at 220-230 nm and a negative dip at 205–215 nm, with both bands dominated by a red-shifted maximum at 195-200 nm, indicative of helix orientation more parallel to the membrane normal. Peptides were at 30 μM, at L/P 100 molar ratios.

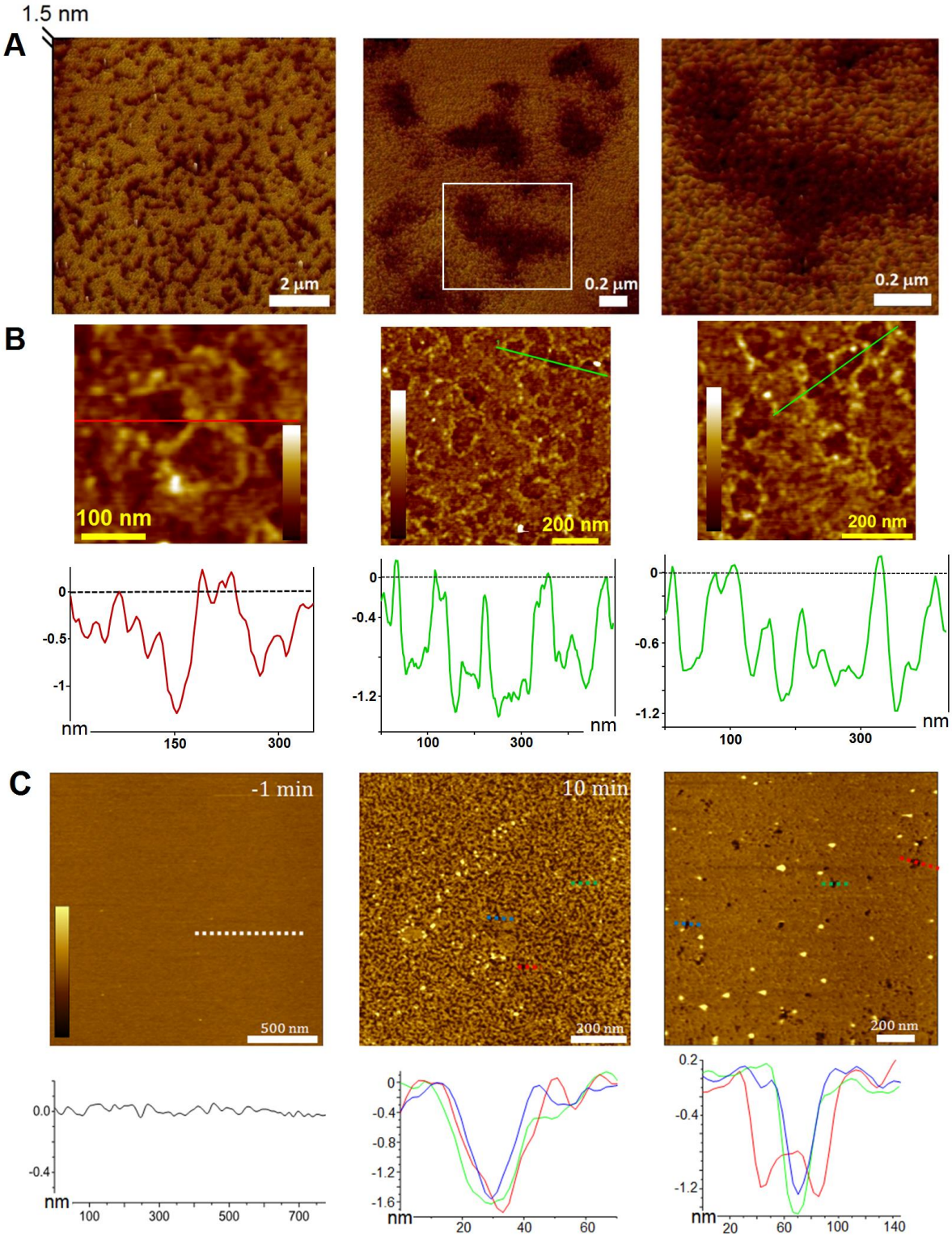

Fig. S5. AFM topography of monolayer poration in supported lipid bilayers. (A) 3D topography of the DLPC/DLPG (3:1, molar ratio) SLBs in aqueous solution incubated (10 min) with tilamin. A higher resolution image corresponding to the area highlighted by a white square is shown on the right. Incubation conditions: 1.8 µM, pH 7.4, rt. (B) In-air topography of the DLPC/DLPG (3:1, molar ratio) SLBs with cross-sections along the highlighted lines. Colour scales: 3 nm. Incubation conditions: 10 µM, pH 7.4, rt. (C) Topography of POPC/POPG (3:1, molar ratio) SLBs in water during incubation (10 min) with tilamin. Cross-sections are along the highlighted lines. Colour scale: 3 nm. Incubation conditions: 1.2 µM, pH 7.4, rt.

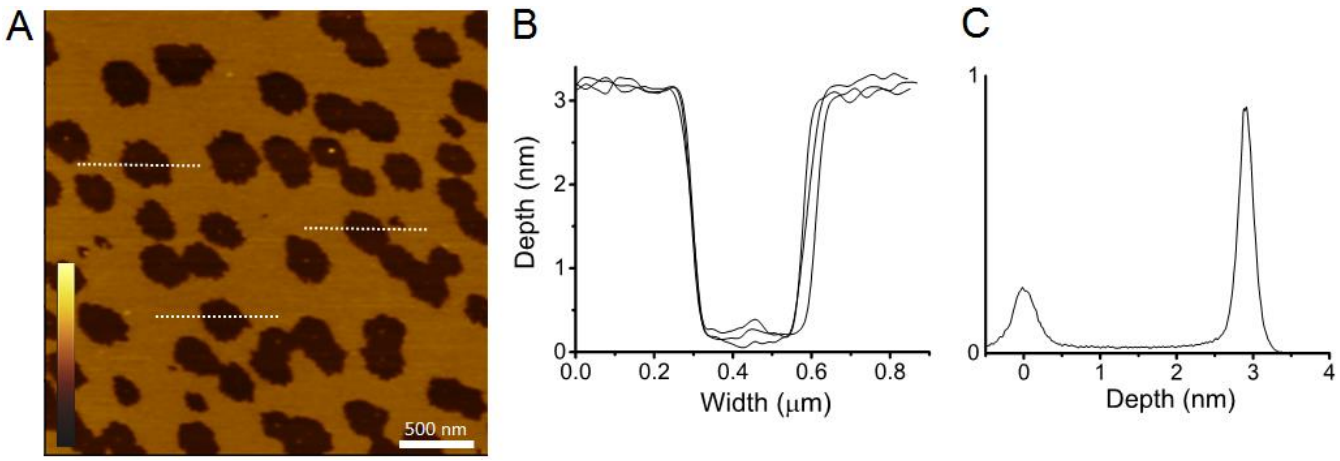

Fig. S6. AFM topography of transmembrane poration by amhelin in supported lipid bilayers. (A) Topography AFM image (20 min) showing expanding transmembrane pores for amhelin (1 μM) in DLPC/DLPG (3:1, molar ratio) SLBs. (B) Cross-section depth profiles along the highlighted lines in (A). (C) Relative occurrence of height values in (A) corresponding to the mica substrate (0 ± 0.2 nm) and the lipid bilayer (3.1± 0.2 nm). Colour scale: 9 nm.

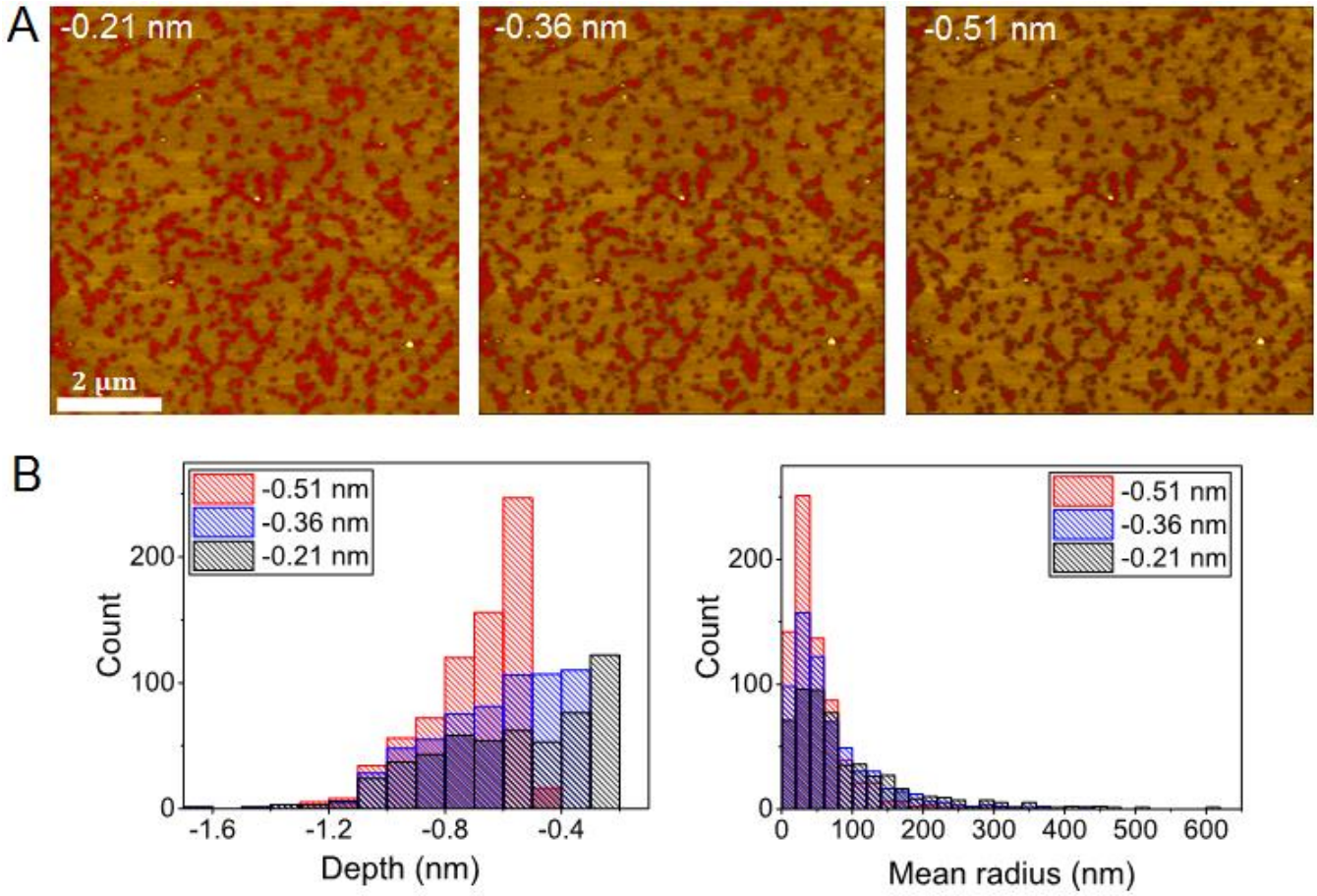

Fig. S7. Quantification of pore size dynamics in supported lipid bilayers. (A) Topography of DLPC/DLPG (3:1, molar ratio) SLBs measured by AFM in aqueous solution during incubation with tilamin (10 min). The pores in the image were measured at three threshold levels set at the heights of -0.21, -0.36 and -0.51 nm with respect to the SLB surface (0 nm). Pores at each threshold level were masked (red) and only areas below the level were measured to give the statistical distributions of pore sizes (B).

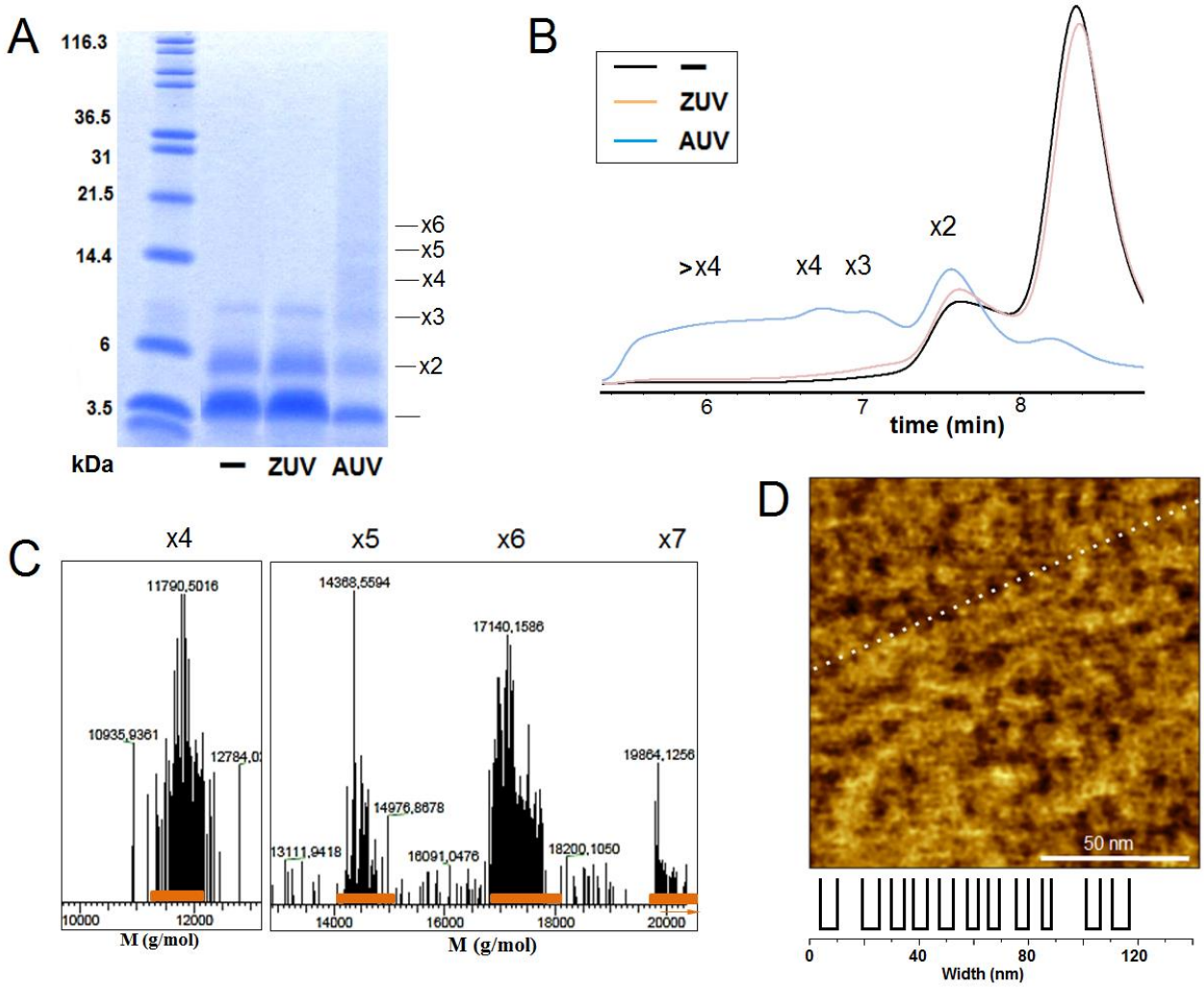

Fig. S8. Comparative mass analysis of tilamin subjected to amine-specific cross-linking. SDS gel electrophoresis (A) and size exclusion chromatography profiles recorded at 215 nm (B) for tilamin cross-linked in buffer (-), DLPC and DLPC/DLPG (3:1, molar ratio) AUVs. Band and peak positions for different oligomers are shown (x2 – >x4). (C) Cross-linked oligomers detected by LC-MS for tilamin in the AUVs with orange bars indicating mass ranges expected for different assembly sizes. (D) Topographic AFM image showing the smallest detected pores for tilamin (1 µM) in DLPC/DLPG (3:1, molar ratio) SLBs with a bar code corresponding to individual pore widths along the highlighted line (compare with Fig S3D).

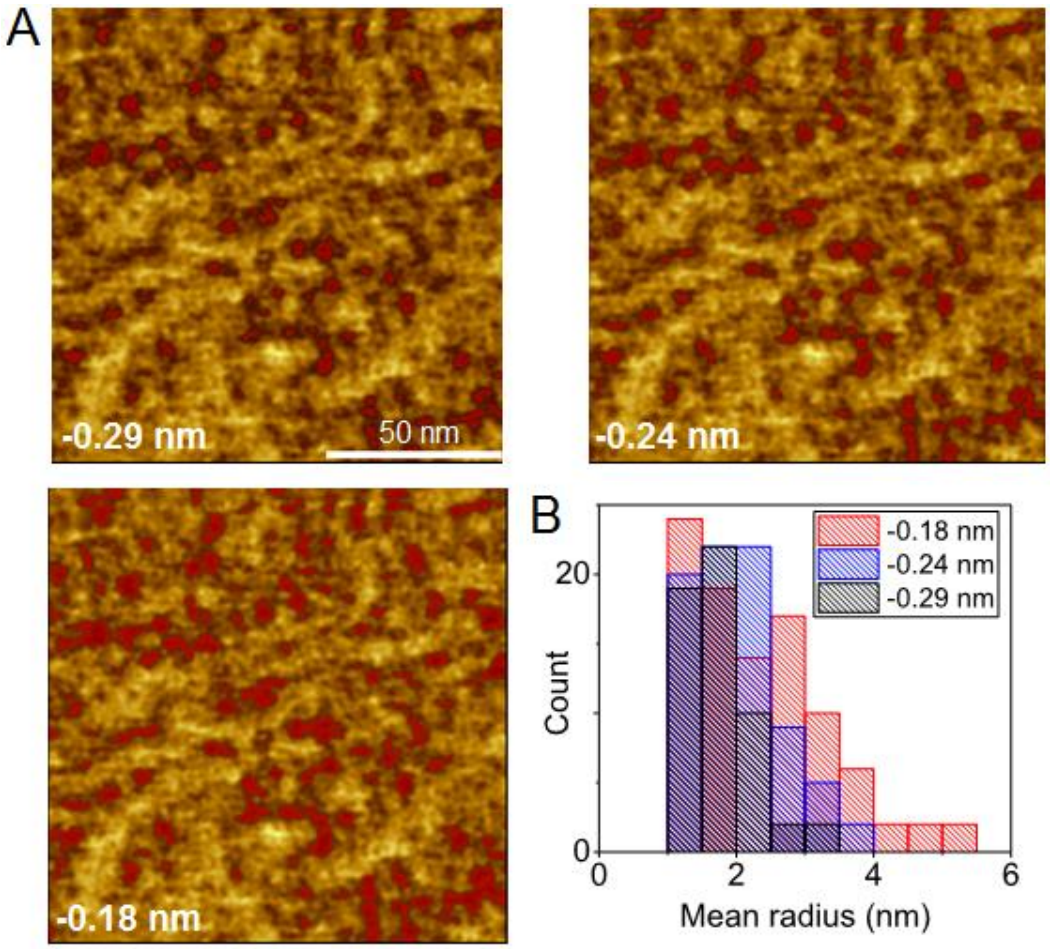

Fig. S9. Quantification of smallest pore size dynamics in supported lipid bilayers. (A) Topography of DLPC/DLPG (3:1, molar ratio) SLBs measured by AFM in aqueous solution during incubation with tilamin (10 min). The pores in the image were measured at three threshold levels set at the heights of -0.18, -0.24 and -0.29 nm with respect to the SLB surface (0 nm). Pores at each threshold level were masked (red) and only areas below the level were measured to give the statistical distributions of pore sizes (B).

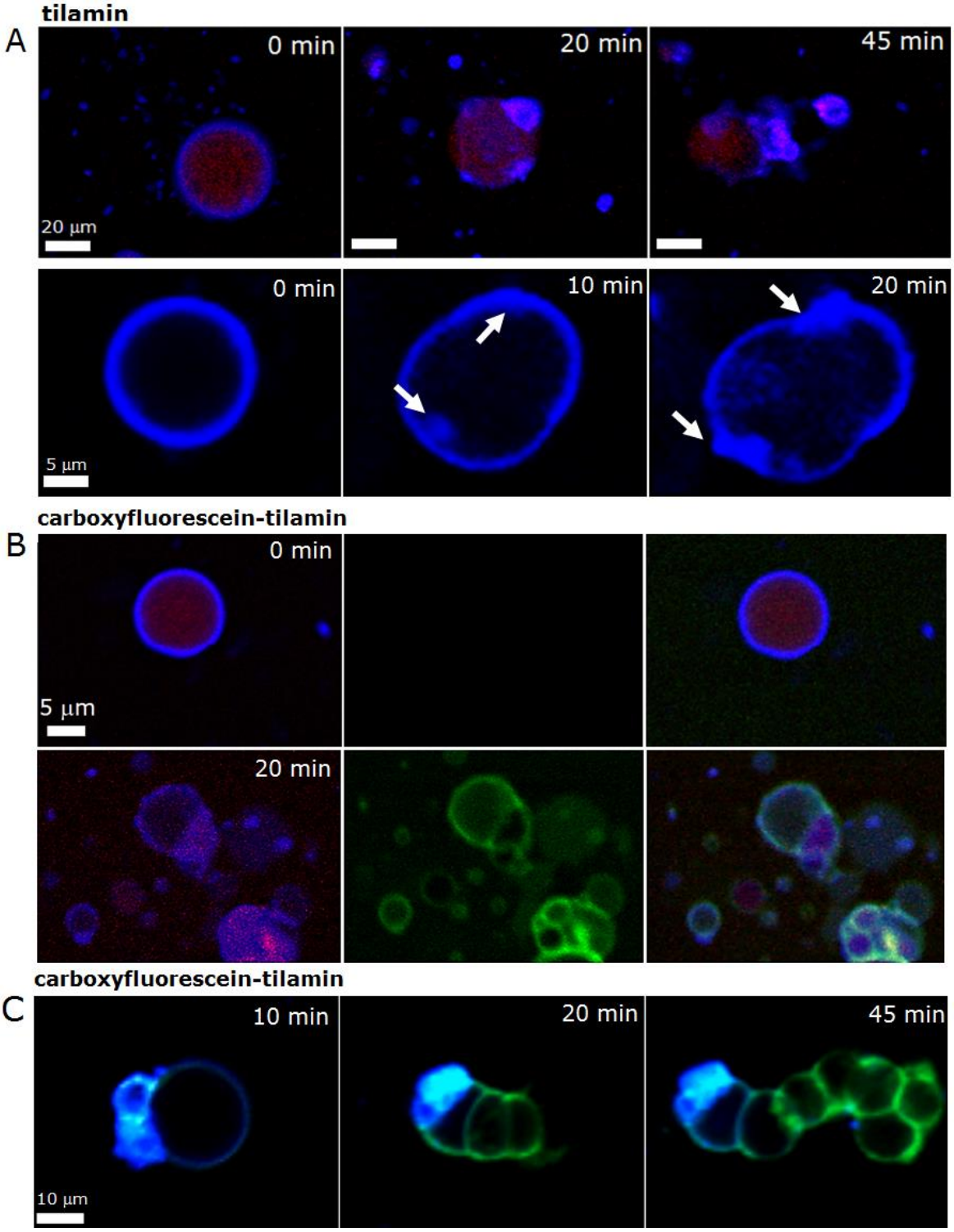

Fig S10. Real-time monitoring of giant unilamellar vesicles (GUVs). Fluorescence micrograph of GUVs assembled from POPC/POPG (3:1, molar ratio) and incubated in PBS with tilamin (10 µM). Key: violet is CellMask^{TM} Deep Red staining GUV membranes, red is sulforhodamine B staining the interior of the GUVs and green is for carboxyfluorescein-labelled tilamin. White arrows point to budding domains. In (B) appropriate filters were used for CellMask^{TM} and sulforhodamine B (left), carboxyfluorescein (middle) and for all three dyes (right). In A (lower) and C sulforhodamine B is omitted for clarity. See also corresponding Video S1 (Fig 4, upper), Video S2 (Fig S7A, upper) and Video S3 (Fig 4, lower).

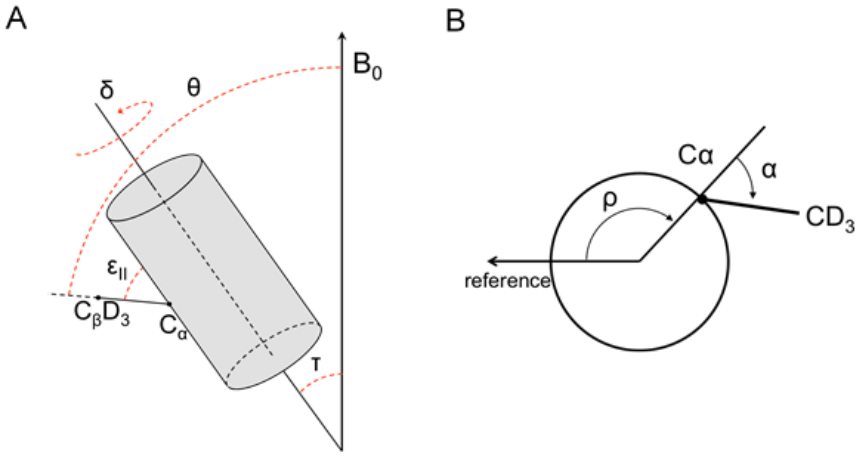

Fig S11. GALA schematic showing (**A**) relevant angles and their relationship to the magnetic field (B_0); (**B**) Geometric description of the overall rotational constraint δ showing angular considerations (top view on a helix).[43]

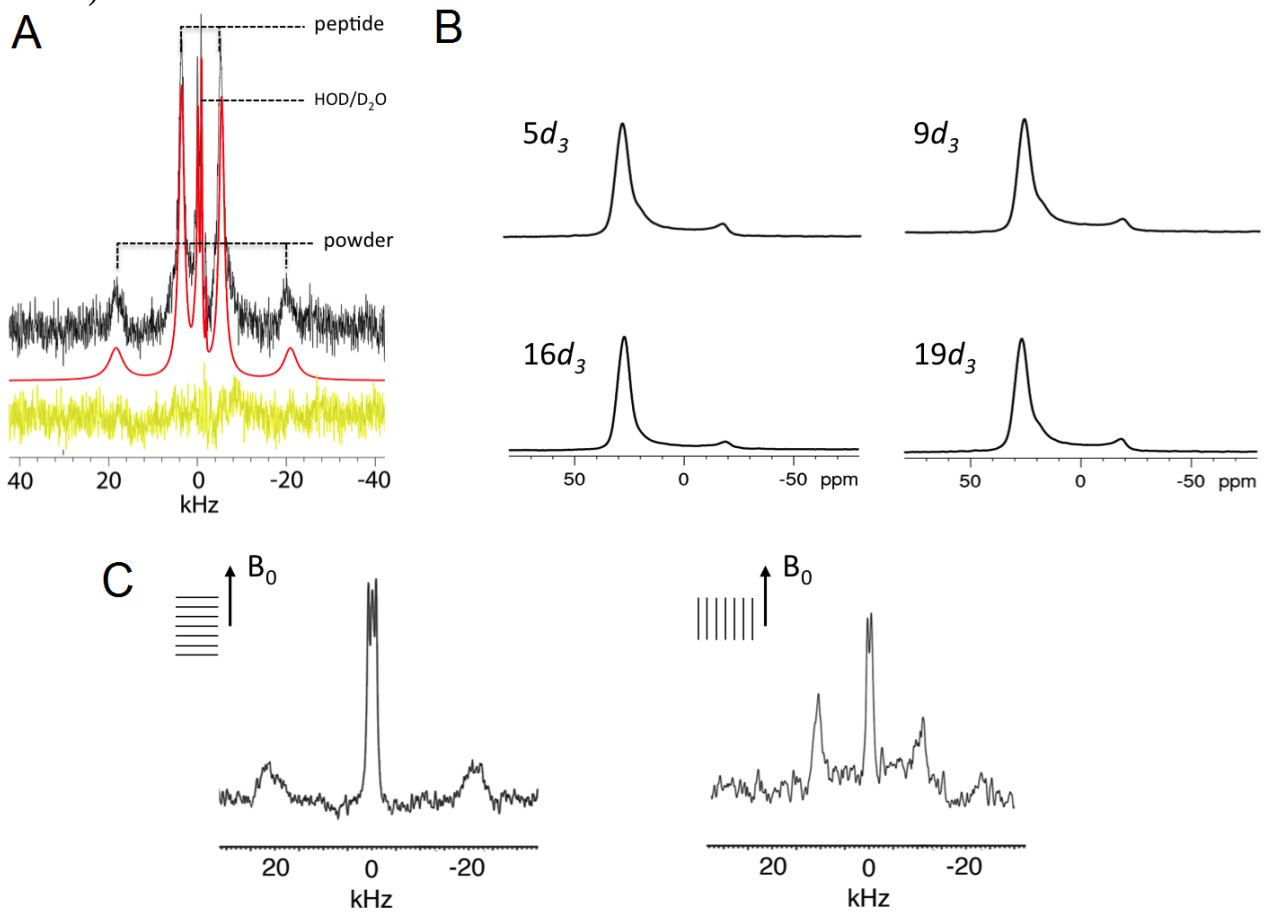

Fig S12. Deconvolution of NMR spectra. (A) Schematic illustration of the deconvolution process of ^{2}H NMR spectra, with the original spectrum shown in black, the deconvoluted spectrum in red and the residuals in yellow. (B) ^{31}P spectra for tilamin deuterated (Ala-d_3) at positions 19, 16, 9, 5 at L/P ratio 25 in POPC/POPG (3:1, molar ratio), corresponding to ^{2}H spectra in Fig 4, showing good sample alignment for all peptide samples. (C) Comparison between tilamin-16d_3 oriented with the bilayer normal parallel (left) and orthogonal (right) to B_0 at L/P ratio 100 in POPC/POPG (3:1, molar ratio). Within the experimental error the quadrupolar splitting halved from 40.8 kHz to 21.1 kHz indicating fast rotational diffusion around the bilayer normal.[S19]

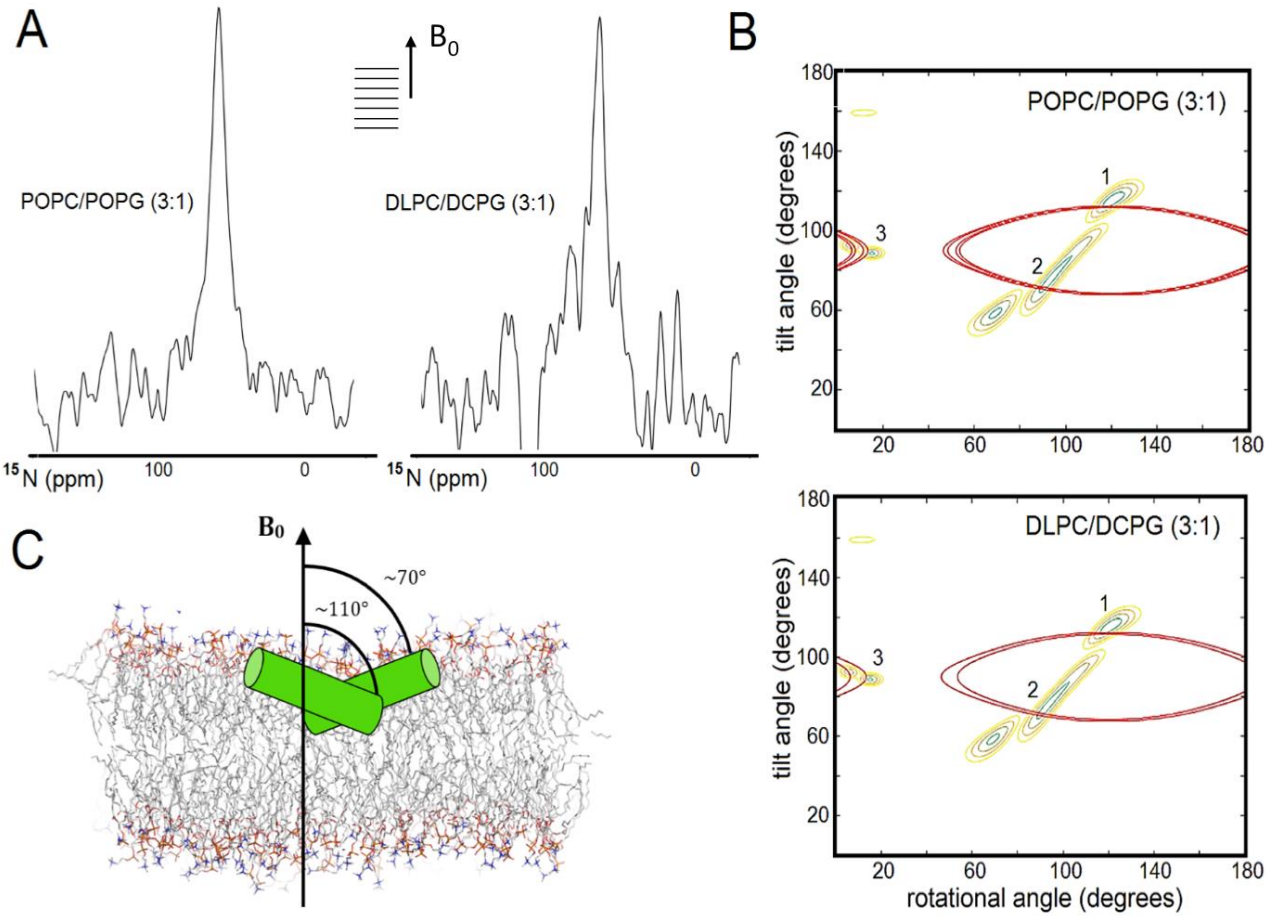

Fig. S13. Tilamin tilting in lipid bilayers. (A) ^{15}N spectra for tilamin labelled at the tyrosine residue in POPC/POPG (3:1, molar ratio) membranes at ~72 ppm (left) and DLPC/DLPG (3:1, molar ratio) membranes at ~75 ppm, with line widths of 14 and 15 ppm respectively. (B) RMSD plots combining the ^{2}H and ^{15}N data. Constraints obtained by ^{15}N are in red. ^{2}H constraints are shown by contour lines for 7 kHz (yellow), 6 kHz (orange), 5 kHz (brown) and 4 kHz (green) in both membrane types. Number 1-3 denote overlapping regions. (C) Orientations of the two answers (1 and 2) in Table S4, which are in agreement with both ^{2}H and ^{15}N experimental data, are shown relative to B_0 in a model palmitoyl bilayer.

Note: Solutions 1 and 2 show nearly identical tilts relative to the bilayer plane, with solution 1 tilting into the bilayer by ~21° and solution 2 by ~20° (Table S4). Solution 3 is also reported despite only a partial overlap in the RMSD plot. This solution is unlikely as the comparable small rotational angle would expose the hydrophobic leucine cluster to the side of the bilayer that is accessible to water. Solutions 1 (110°) and 2 (70°) are nearly identical in terms of the tilt relative to the bilayer plane, which makes helix insertion by the N- or C-terminus equally possible. The inserting end of tilamin for solution 1 is the N-terminus, whereas for solution 2 it is reversed (Table S4).

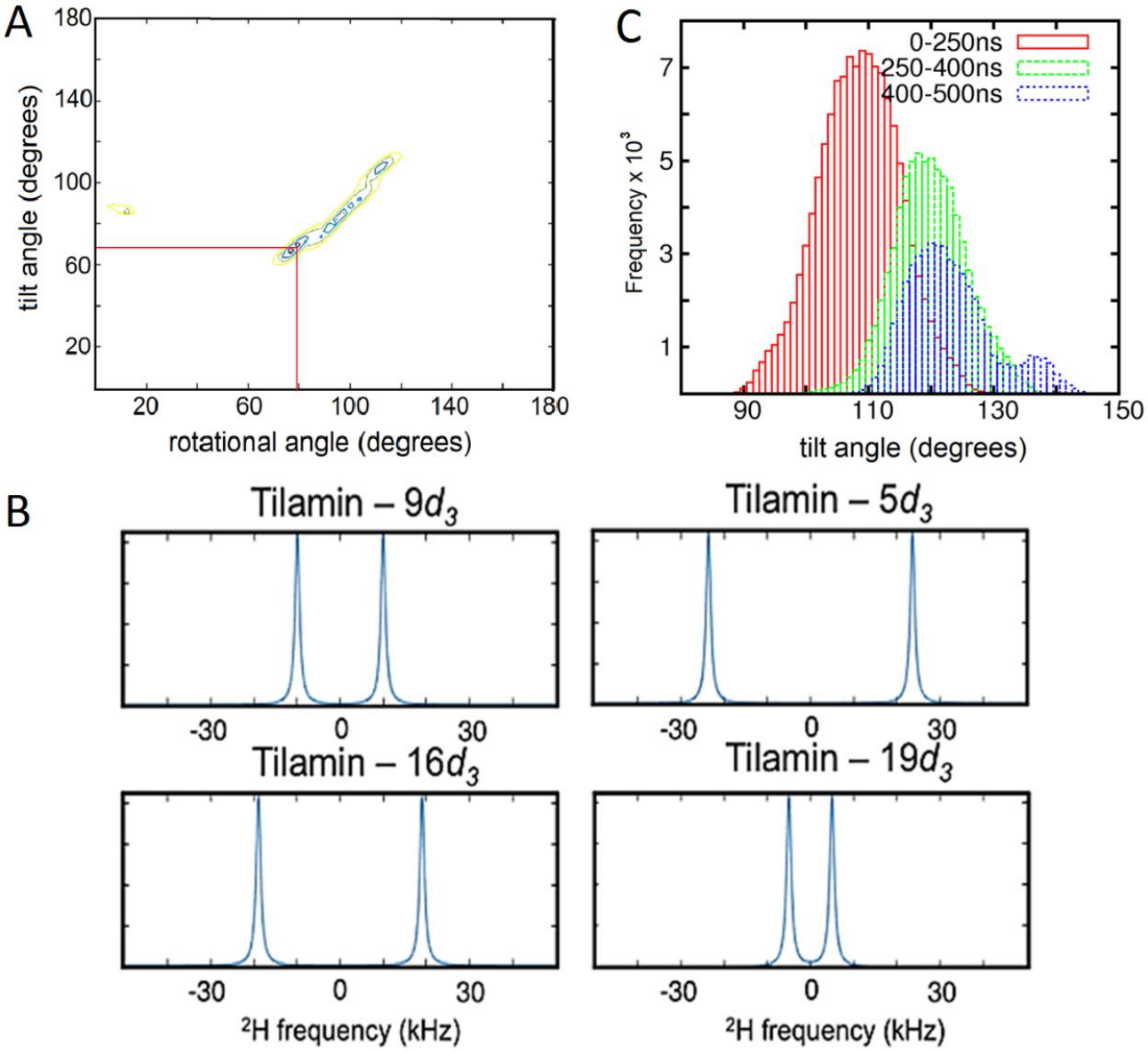

Fig. S14. Simulated tilamin tilting in lipid bilayers. (A) RMSD plot of simulated ^{2}H NMR spectra. The contour levels show RMSD values of 2, 3, 4 and 5 kHz. The closest fit (RMSD 1.1 kHz) is illustrated. (B) Simulated ^{2}H NMR spectra for the lowest RMSD value for all of ^{2}H constraints used (absolute values are shown in Table S5). (C) The distribution of helix tilt angles relative to the membrane normal for a single tilamin helix inserted into a dilauroyl (DLPC/DLPG, 3:1 molar ratio) bilayer at different stages of the MD simulation.

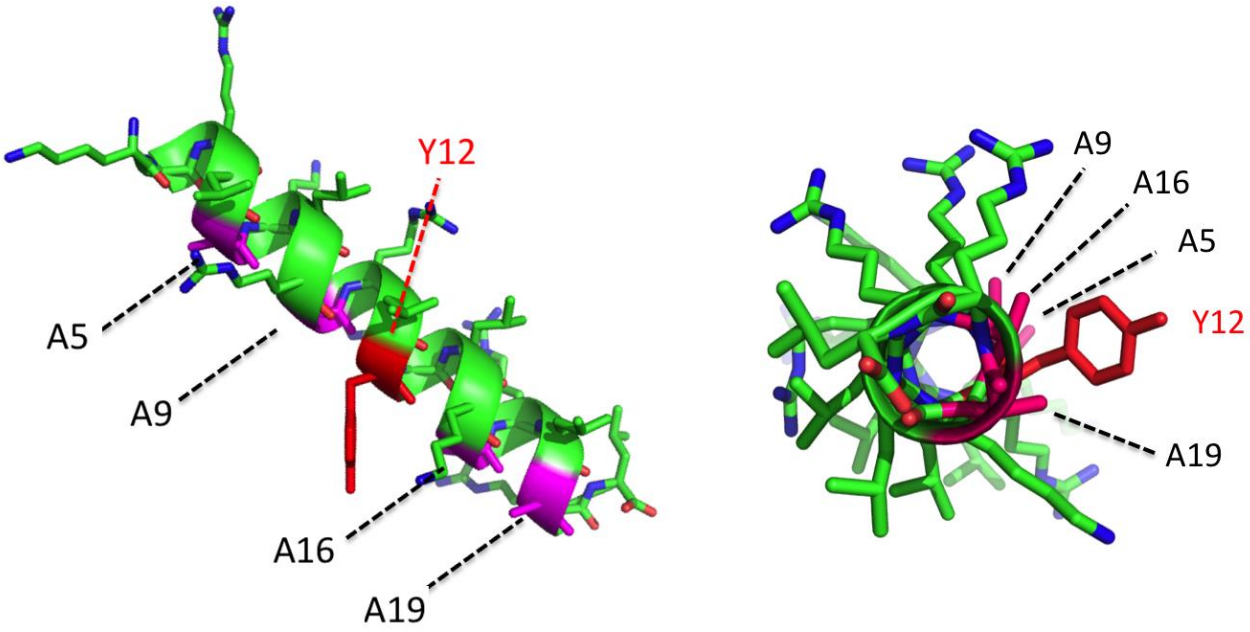

Fig. S15. Relative positions of labelled amino acids in the tilamin helix. GALA- and MD-derived tilamin helix tilt (left) and a helix bottom-up view (right) showing label positions 5, 9, 12, 15 and 19 (Ala-d_3 shown in magenta and Tyr-^{15}N in red). The helices are not to scale. The helix insertion by the C-terminus (Solution 2) is shown (Table S4).

Notes for estimated relationships between tilamin tilt and pore dimensions: upon binding to membranes the tilamin folds into a helix of 3.15 nm in length. At tilts of 70°, 60° and 50° (or 110°, 120° and 130°) with respect to the membrane normal the tilamin helix is a hypotenuse that forms a right-angled triangle with the catheti of membrane normal and the membrane plane. Knowing the length of the hypotenuse (3.15 nm) and its adjacent angles (i.e. 70° and 20°, 60° and 30°, 50° and 40°), both catheti can be calculated to give:

- insertion depths (membrane normal cathetus) at 1.1, 1.6 and 2 nm, respectively, which match the pore depths of 1.2-1.8 nm observed by microscopy (Fig 6B), and
- the span of the tilted helix (as a projection of the membrane plane cathetus) of 2.4-3 nm, which constitutes a half of a minimal pore facing an opposite helix – i.e. 5-6 nm, consistent with the smallest pores of 5-10 nm (Fig S8D).

Peptide cross-linking followed by mass-spectrometric, chromatographic and electrophoretic analyses revealed oligomeric forms consisting of 4-7 tilamin molecules (Fig S8A-C). To cross-link, these molecules must be in the proximity of <11.4 Å to each other – the length of the cross-linking reagent used, while an average intermolecular distance of ~160 Å is expected in solution under the same conditions (see **Tilamin cross-linking**). Thus, the smallest pores with the outlined dimensions are low-oligomer pores as simulated in Fig 6C.

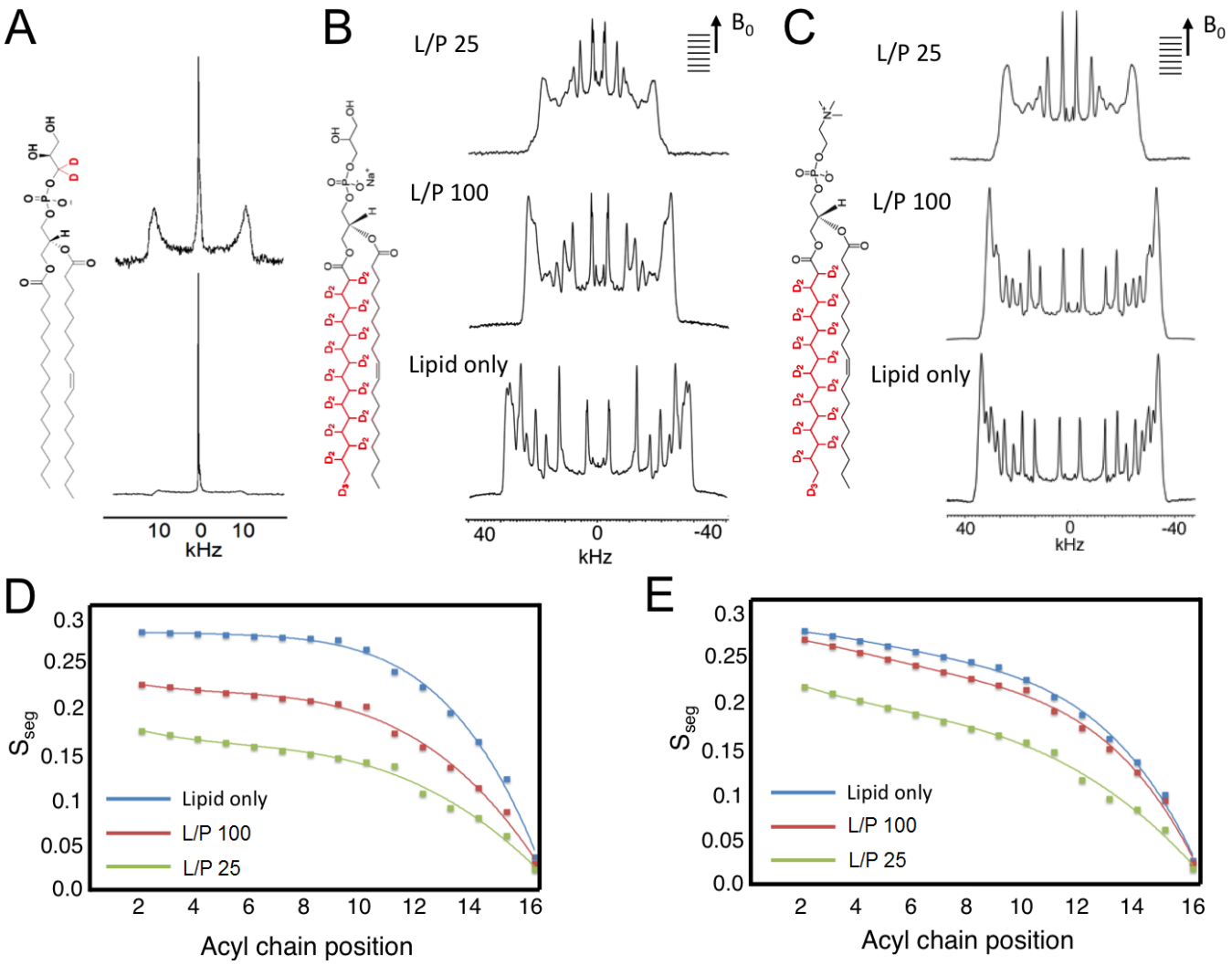

Fig. S16. Tilamin charge interplays upon insertion. (A) ssNMR spectra of unlabelled tilamin in deuterated POPC/POPG-d_2 membranes (3:1, molar ratio; dispersion and de-Paked to simulate oriented spectra) showing the complete disruption of headgroup regions (POPG-d2) in the presence of tilamin (lower) at L/P 100 ratio when compared to lipid only spectra (upper). The chemical structure of POPG-d_2 (deuterated positions in red) are shown next to the spectra. (B, C) ssNMR spectra of unlabelled tilamin in deuterated (B) POPC/POPG-d_{31} and (C) POPC-d_{31}/POPG (3:1, molar ratio; mechanically aligned) membranes showing the partial disruption of quadrupolar splittings. The chemical structure of POPG-d_{31} (deuterated positions in red) are shown next to the spectra, the same positions are for POPC-d_{31}. (D, E) Segmental order parameters (*Sseq*) calculated from quadrupolar splittings of acyl chain deuterated lipids plotted as a function of chain position POPG-d_{31} (D) and POPC-d_{31} (E). Collectively, the data is consistent with tilamin having a greater disordering impact on the anionic POPG component (POPG-d_2, POPG-d_{31}).

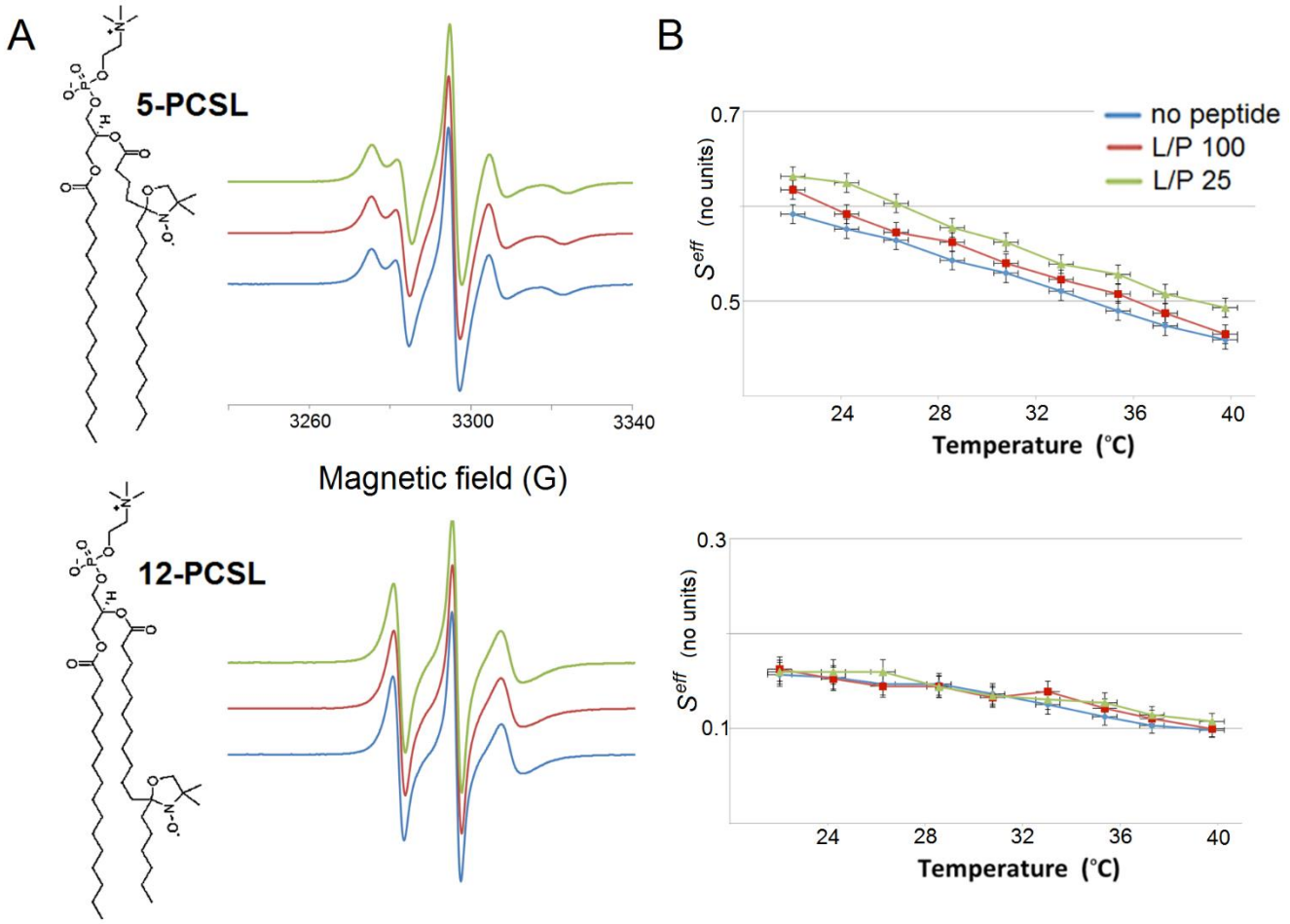

Fig. S17. Tilamin charge interplays upon insertion. (A) Segmental acyl chain motion upon tilamin binding as probed with nitroxide labelled lipids POPC/POPG (3:1, molar ratio) by continuous wave electron paramagnetic resonance at different lipid-peptide ratios: green (25), red (100) and blue (no peptide). Chemical structures of spin-labelled probes (phosphatidylcholine with the nitroxide spin label at positions 5 (5-PCSL) (upper) and 12 (12-PCSL) (lower) of the acyl chain) are shown. (B) Segmental order parameters (S^{eff}) calculated for the probed segments 5-PCSL (upper) and 12-PCSL (lower) and plotted versus temperature. With fast molecular motions on the EPR timescale (ns) the anisotropy of the nitroxide spin label is expressed as an order parameter describing angular amplitude of motion at the labelled position.

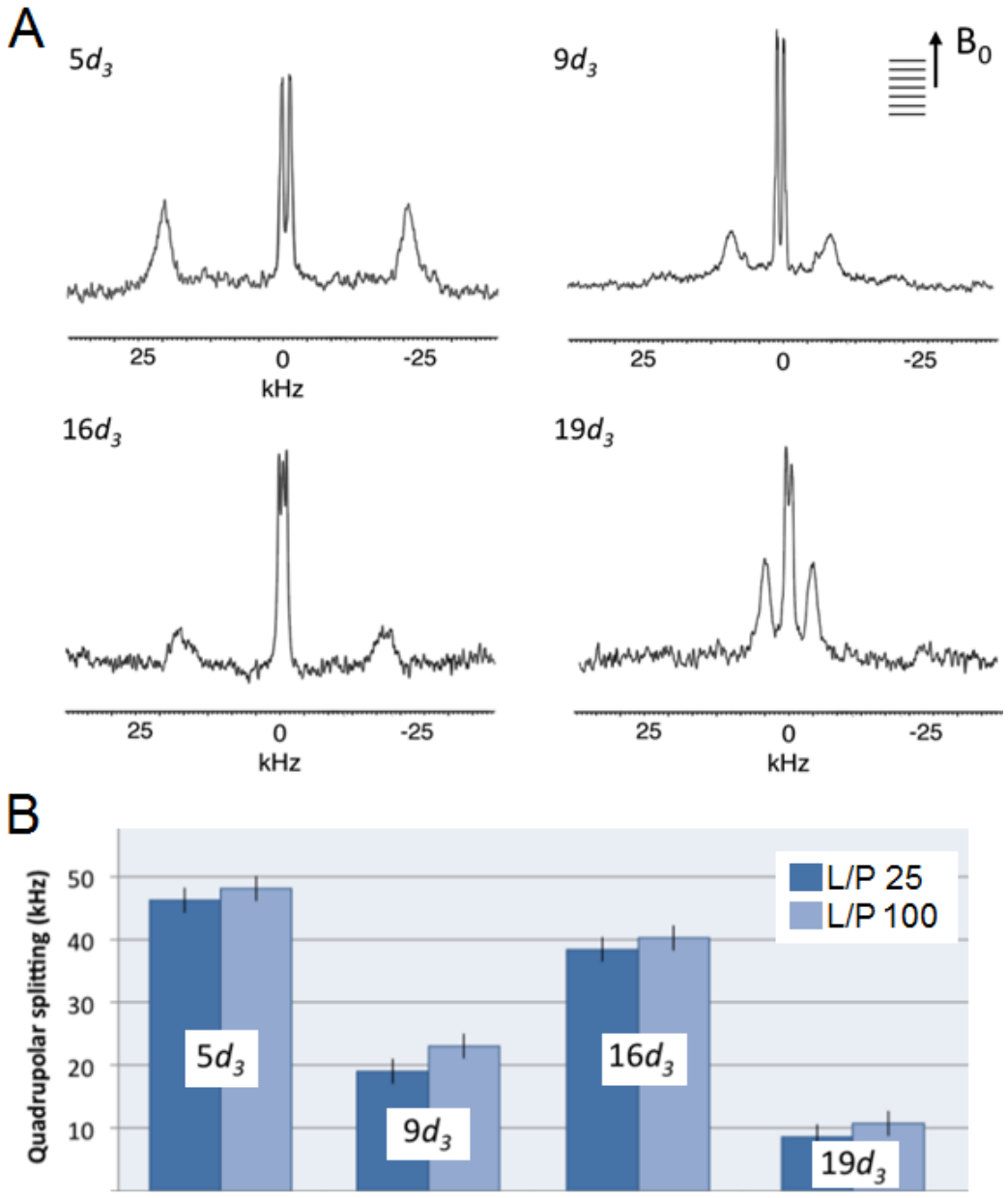

Fig. S18. Tilamin insertion mode. (A) Oriented ^{2}H NMR quadrupolar splittings (ΔνQ) in palmitoyl (POPC/POPG, 3:1 molar ratio) membranes for tilamin deuterated (Ala-d_3) at positions 19, 16, 9, 5 at L/P ratio 100. (B) Chart comparing the observed quadrupolar splittings at L/P 25 and 100.

Note: a small, but consistent, increase observed across all deuterated positions with increasing L/P ratios (25 to 100) is attributed to a lower motion of the peptide, and hence less anisotropic averaging of the quadrupolar interaction, in the ordered membrane (Fig S16 D,E) compared to tilamin in a disordered membrane. Absolute splittings are shown in Table S2.

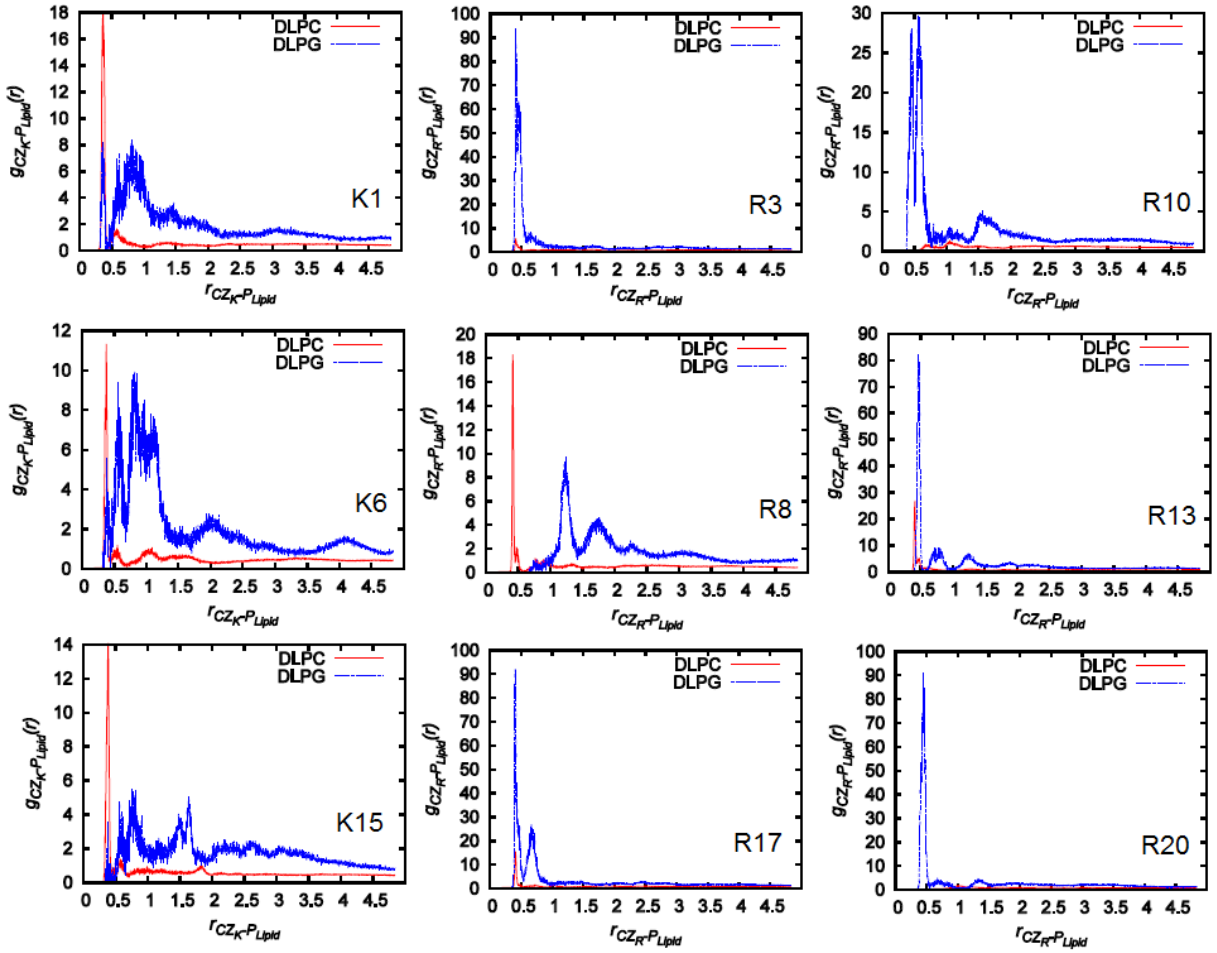

Fig S19. Charge interplays in the bilayer. Normalised rotational distribution functions calculated for charged tilamin sidechains, showing the proximity of DLPC and DPLG phosphate atoms in the final 100 ns of 500-ns atomistic simulations. K1, K6, R8, K15 appear to preferentially bind to the anionic DLPG.

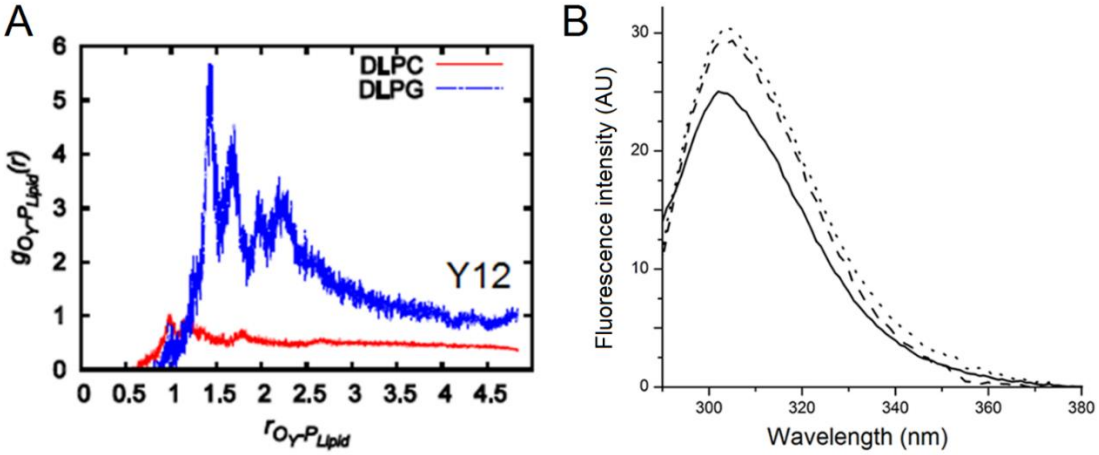

Fig S20. Tyrosine interactions in the bilayer. (A) Normalised rotational distribution functions calculated for the tyrosine side chain, showing the proximity of DLPC and DPLG phosphate atoms in the final 100 ns of 500-ns atomistic simulations. (**B**) Fluorescence spectra of tilamin (15 µM) in phosphate buffer (solid line) and in the presence of DLPC/DLPG (3:1, molar ratio) (dotted line) and POPC/POPG (3:1, molar ratio) (dashed line) membranes.

References

S1. N. Das, D. T. Murray, T. A. Cross, *Nat Protocols* 2013, **8,** 2256.
S2. P. L. Gor'kov *et al. J Magn Reson* 2007, **185,** 77.
S3. E. Strandberg, S. Esteban-Martín, J. Salgado, A. S. Ulrich, *Biophys. J.* 2009, **96,** 3223.
S4. K. Bertelsen *et al. J Am Chem Soc* 2007, **129,** 14717.
S5. E. Strandberg *et al. Biochemistry* 2008, **47,** 2601.
S6. A. Pines, M. G. Gibby, J. S. Waugh, *J Chem Phys* 1973, **59,** 569.
S7. A. Bechinger, C. Aisenbrey, P. Bertani, *Biochim. Biophys. Acta* 2004, **1666,** 190.
S8. T. G. Oas, C. J. Hartzell, F. W. Dahlquist, G. P. Drobny, *J. Am. Chem. Soc.* 1987, **109,** 5962.
S9. H.J. Hogben *et al. J Magn Reson*, **208** 179-194 (2011).
S10. M.-A. Sani, D. K. Weber, F. Delaglio, F. Separovic, J. D. Gehman, *PeerJ* 2013, **1,** e30.
S11. D. Lu, I. Vavasour, M. R. Morrow, *Biophys. J*, **68**, 574–583 (1995).
S12. E. S. Salnikov *et al.* in *Adv. Biol. Solid-State NMR*, (F. Separovic & A. Naito, eds.), Cambridge, RSC Publishing (2014).
S13. D. Marsh, A. Watts, in *Liposomes: from physical structure to therapeutic applications.* (1981)
S14. P. Jost, L. J. Libertini, V. C. Hebert, O. H. Griffith, *J. Mol. Biol.* 1971, **59,** 77.
S15. Y. Qi, Y. *et al. J. Chem. Theory Comput.* 2015, **11,** 4486.
S16. D. H. de Jong *et al. J. Chem. Theory Comput.* 2012, **9,** 687.
S17. S. Pronk, S. *et al. Bioinformatics* 2013, **29,** btt055–854.
S18. W. Humphrey, A. Dalke, K. Schulten, *J Mol Graph* 1996, **14,** 33.
S19. C. Aisenbrey, B. Bechinger, *J Am Chem. Soc.* 2004, **126**, 16676.